Design, Formation and Properties of Tetrahedral M_4L_4 and M_4L_6 Supramolecular Clusters[1]

Dana L. Caulder, Christian Brückner, Ryan E. Powers, Stefan König, Tatjana N. Parac, Julie A. Leary, and Kenneth N. Raymond*

Contribution from the Department of Chemistry, University of California, Berkeley, California 94720-1460

Received February 20, 2001

Abstract: The rigid tris- and bis(catecholamide) ligands H_6**A**, H_4**B** and H_4**C** form tetrahedral clusters of the type M_4L_4 and M_4L_6 through self-assembly reactions with tri- and tetravalent metal ions such as Ga^{III}, Fe^{III}, Ti^{IV} and Sn^{IV}. General design principles for the synthesis of such clusters are presented with an emphasis on geometric requirements and kinetic and thermodynamic considerations. The solution and solid-state characterization of these complexes is presented, and their dynamic solution behavior is described. The tris-catecholamide H_6**A** forms M_4L_4 tetrahedra with Ga^{III}, Ti^{IV}, and Sn^{IV}; $(Et_3N)_8[Ti_4\mathbf{A}_4]$ crystallizes in $R\bar{3}c$ (No. 167), with a = 22.6143(5) Å, c = 106.038(2) Å. The cluster is a racemic mixture of homoconfigurational tetrahedra (all Δ or all Λ at the metal centers within a given cluster). Though the synthetic procedure for synthesis of the cluster is markedly metal-dependent, extensive electrospray mass spectrometry investigations show that the $M_4\mathbf{A}_4$ (M = Ga^{III}, Ti^{IV}, and Sn^{IV}) clusters are remarkably stable once formed. Two approaches are presented for the formation of M_4L_6 tetrahedral clusters. Of the bis(catecholamide) ligands, H_4**B** forms an M_4L_6 tetrahedron (M = Ga^{III}) based on an "edge-on" design, while H_4**C** forms an M_4L_6 tetrahedron (M = Ga^{III}, Fe^{III}) based on a "face-on" strategy. $K_5[Et_4N]_7[Fe_4\mathbf{C}_6]$ crystallizes in $I\bar{4}3d$ (No. 220) with a = 43.706(8) Å. This M_4L_6 tetrahedral cluster is also a racemic mixture of homoconfigurational tetrahedra and has a cavity large enough to encapsulate a molecule of Et_4N^+. This host−guest interaction is maintained in solution as revealed by NMR investigations of the Ga^{III} complex.

Introduction

Nature provides stunning examples of noncovalently linked molecular clusters of high symmetry. Studied by electron microscopy and X-ray diffraction, the high symmetry of viruses has been recognized since the late 1950s.[2] The protein coat of the human rhinovirus, among others, is composed of 60 copies of each of four protein subunits arranged in icosahedral symmetry.[2,3] Viral protein coats are not the only high-symmetry natural clusters, however. The Fe-storage protein ferritin is composed of 24 identical protein subunits arranged in octahedral symmetry.[4] Interestingly, in most cases these clusters spontaneously self-assemble from their identical subunits. Particularly enticing is the fact that these high-symmetry structures are utilized as protective shells: The virus coats protect genetic material, while the ferritin shell stores several thousand iron atoms as polymeric ferric oxy hydroxide.

Under the assumption that evolutionary pressure drove optimization of the shell design, rationales have been put forward to explain the frequent occurrence of such self-assembled structures. Subunit economy concomitant with maximization of the enclosed space and mechanical rigidity of the resulting structure have been cited in reference to the viral protein coats.[2] As little as one gene is required to encode the protein that in turn contains all of the information necessary for multiple copies of the protein to self-assemble into the complete shell. This remarkable economy makes the synthesis of artificial shells by the self-assembly of a large number of small and simple subunits an attractive goal, particularly in view of the rather involved syntheses often required for the generation of even small molecular containers.[5,6] Thus, current trends toward the utilization of self-assembling identical subunits are not surprising.[7−9]

While the individual interactions holding protein subunits together (e.g., H-bonds, van der Waals interactions, and $\pi-\pi$ interactions) have been recognized, it is less understood what algorithms direct the synergy of these interactions to form exclusively the observed clusters. An understanding of the natural algorithms utilized to induce a single stoichiometry and symmetry rather than a variety of oligomers and polymers should lead to the deduction of general design principles for synthetic self-assembled structures. Attempts have been made to illustrate mathematically the underlying geometric implications for a subunit capable of forming such closed-shell suprastructures.[2,10] Viruses have been suggested as models for new supramolecular architectures without, however, providing explicit building instructions.[11] We have suggested the utilization of a symmetry-based model for the synthesis of supramolecular

(1) Coordination Number Incommensurate Cluster Formation, Part 21. For the previous paper in this series, see Sun, X.; Johnson, D. W.; Raymond, K. N.; Wong, E. H., *Inorg. Chem.* **2001**, *40*, 4504−4506.

(2) Caspar, D. L. D.; Klug, A. *Cold Spring Harbor Symposia on Quantitative Biology*; Long Island Biological Association: New York, 1962; Vol. 27, pp 1−24.

(3) (a) Arnold, E.; Rossmann, M. G. *Acta Crystallogr., Sect. A.* **1988**, *44*, 270−282. (b) The Universal Virus Database: http://www.ncbi.nlm.nih.gov/ICTVdb/welcome.htm.

(4) Harrison, P. M.; Arosio, P. *Biochim. Biophys. Acta* **1996**, *1275*, 161−203.

(5) Cram, D. J.; Cram, J. M. *Container Molecules and their Guests*; Royal Society of Chemistry: Cambridge, 1994; Vol. 4.

(6) Jasat, A.; Sherman, J. C. *Chem. Rev.* **1999**, *99*, 931−968.

(7) Böhmer, V. *Angew. Chem., Int. Ed. Engl.* **1995**, *34*, 713−745.

(8) (a) Martin, T.; Obst, U.; Rebek, J., Jr. *Science* **1998**, *281*, 1842−1845. (b) Rebek, J. J. *Chem. Soc. Rev.* **1996**, *25*, 255−264.

(9) Conn, M. M.; Rebek, J., Jr. *Chem. Rev.* **1997**, *97*, 1647−1668.

10.1021/ja0104507 CCC: $20.00
Published on Web 08/23/2001

clusters by using metal−ligand interactions to generate the required symmetries. This building principle, "the coordination number incommensurate cluster formation model," provides guidelines for the rational design of symmetric clusters, the larger of which have well-defined cavities.[12] The great utility of such cavities has been shown by the chemistry made possible in the "inner phase" of calixarenes, carceplexes, and other host molecules.[6] This is paralleled by the formation of polyoxometalates in the hollow interior of a virus purged of its RNA genetic material.[13] Future growth of the field of nanotechnology depends on reliable and predictable container compounds.

The utilization of H-bonds for the construction of molecular clusters has resulted in spectacular supramolecular structures,[8,9,14] but the use of the stronger, highly directional and well-studied metal−ligand interaction has also afforded discrete clusters of a variety of sizes, stoichiometries, and symmetries. Although early work has focused on the synthesis of helicates, the wide structural flexibility of coordination chemistry has made possible the realization of boxes, grids, rings, tetrahedra, cubes, rotaxanes, and catenates.[9,12,15,16]

While there are numerous accounts of the synthesis of M_4L_x-type ($x = 4,6$) tetrahedra, their syntheses have, at least initially, relied on fortuitous circumstance.[17] Few early reports detailed underlying design principles, despite the fact that supramolecular chemistry has been described as a kind of molecular information science,[16] which implies that the instructions "programmed" into each component of an assembly direct the formation of a distinct cluster topology. If this is indeed the case, *then the compilation of the information required to instruct components to self-assemble into a predictable cluster should be the starting point of all synthetic efforts*. In practicality, this means that the design of components in which the information for the formation of a cluster is inherent should begin the synthesis of a supramolecular cluster. Second, the required reaction conditions necessary for the successful assembly of the cluster should be evaluated. In a sense this sequence is standard procedure in organic synthesis when planning a target-oriented synthesis by means of retrosynthetic analysis.[18]

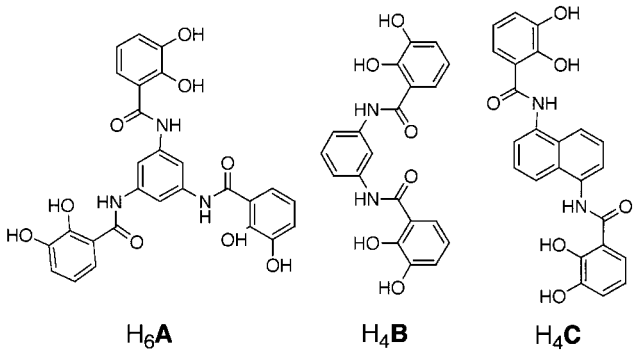

H_6**A** H_4**B** H_4**C**

Figure 1. Ligands H_6**A**, H_4**B**, and H_4**C** form tetrahedral clusters with tri- and tetravalent metal ions.

It is the goal of this series of papers to develop a symmetry-based set of principles for the rational design and synthesis of supramolecular clusters. In this paper, examples for the synthesis and analysis of M_4L_x-type ($x = 4,6$) tetrahedra built using three different design approaches will be provided. In particular, the design, synthesis, and solution- and solid-state characterization of tetrahedral clusters based on ligands H_6**A**, H_4**B**, and H_4**C** (Figure 1) will be discussed. The design principles delineated here are conceived to be general and transferable to the design of metal−ligand clusters of varying symmetries, sizes, and compositions.

General Principles for the Formation of Metal−Ligand-Based Clusters. When planning the synthesis of clusters based on metal−ligand interactions, the general choice of ligand type, ligand backbone rigidity, metal type, and reaction conditions have to be considered. The particular geometric requirements for each cluster's symmetry and stoichiometry have to be strictly fulfilled, since it is the metal-coordination geometry and the orientation of the interaction sites in any given ligand that provide the inherent information, or blueprint, for the self-assembly of a designed cluster. We will discuss each point of consideration separately, starting from more general requirements and followed by the design principles for the synthesis of particular cluster symmetries. Finally, the synthesis, structural characterization, and solution chemistry of tetrahedral M_4L_x ($x = 4,6$) clusters will be detailed.

Choice of a Metal−Ligand Combination. The driving force for the formation of the cluster is derived from metal−ligand interactions. Thus, the choice of relatively strong metal-binding moieties, for example, chelating moieties, is preferred. (Although, a number of large clusters based on the interaction of monodentate amine- or pyridine-type donors with Pt^{II} and Pd^{II} are known.[19]) The self-assembly product should be the thermodynamically favored cluster (for further thermodynamic considerations, see below); however, kinetic products such as nonstoichiometric oligomers and polymers will be formed at

(10) (a) Raymond, K. N.; Caulder, D. L.; Powers, R. E.; Beissel, T.; Meyer, M.; Kersting, B. *Proc. of the 40th Robert A. Welch Found. on Chem. Res.* **1996**, *40*, 115−129. (b) Olenyuk, B.; Levin, M. D.; Whiteford, J. A.; Shield, J. E.; Stang, P. J. *J. Am. Chem. Soc.* **1999**, *121*, 10434−10435. (c) MacGillivray, L. R.; Atwood, J. L. *Angew. Chem., Int. Ed.* **1999**, *38*, 1018−1033. (d) Albrecht, M. *Angew. Chem., Int. Ed.* **1999**, *38*, 3463−3465.

(11) Percec, V. *J. Macromol. Sci., Pure Appl. Chem.* **1996**, *A33*, 1479−1496.

(12) (a) Caulder, D. L.; Raymond, K. N. *J. Chem. Soc., Dalton Trans.* **1999**, 1185−1200. (b) Caulder, D. L.; Raymond, K. N. *Acc. Chem. Res.* **1999**, *32*, 975−982.

(13) Douglas, T.; Young, M. *Nature* **1998**, *393*, 152−155.

(14) (a) Wyler, R.; de Mendoza, J.; Rebek, J., Jr. *Angew. Chem., Int. Ed. Engl.* **1993**, *32*, 1699−1701. (b) Meissner, R. S.; Rebek, J., Jr.; de Mendoza, J. *Science* **1995**, *270*, 1485−1488. (c) Mathias, J. P.; Simanek, E. E.; Seto, C. T.; Whitesides, G. M. *Angew. Chem., Int. Ed. Engl.* **1993**, *32*, 1766−1769. (d) Mascal, M.; Hext, N. M.; Warmuth, R.; Moore, M. H.; Turkenburg, J. P. *Angew. Chem., Int. Ed. Engl.* **1996**, *35*, 2204−2206. (e) MacGillivray, L. R.; Atwood, J. L. *Nature (London)* **1997**, *389*, 469−472. (f) Grotzfeld, R. M.; Branda, N.; Rebek, J., Jr. *Science* **1996**, *271*, 487−489.

(15) (a) Williams, A. F. *Pure Appl. Chem.* **1996**, *68*, 1285−1289. (b) Piguet, C.; Bernardinelli, G.; Hopfgartner, G. *Chem. Rev.* **1997**, *97*, 2005−2062. (c) Jones, C. J. *Chem. Soc. Rev.* **1998**, *27*, 289−299. (d) Sauvage, J. P. *Acc. Chem. Res.* **1998**, *31*, 611−619. (e) Saalfrank, R. W.; Demleitner, B. In *Transition Metals in Supramolecular Chemistry*; Sauvage, J. P., Ed.; Wiley-VCH: Weinheim, 1999; Vol. 5, pp 1−51. (f) Leininger, S.; Olenyuk, B.; Stang, P. J. *Chem. Rev.* **2000**, *100*, 853−907.

(16) Lehn, J.-M. *Supramolecular Chemistry: Concepts and Perspectives*; VCH: Weinheim, 1995.

(17) (a) Saalfrank, R. W.; Stark, A.; Bremer, M.; Hummel, H. *Angew. Chem., Int. Ed. Engl.* **1990**, *29*, 311−314. (b) Saalfrank, R. W.; Horner, B.; Stalke, D.; Salbeck, J. *Angew. Chem., Int. Ed. Engl.* **1993**, *32*, 1179−1182. (c) Saalfrank, R. W.; Burak, R.; Breit, A.; Stalke, D.; Herbst-Irmer, R.; Daub, J.; Porsch, M.; Bill, E.; Müther, M.; Trautwein, A. X. *Angew. Chem., Int. Ed. Engl.* **1994**, *33*, 1621. (d) Saalfrank, R. W.; Burak, R.; Reihs, S.; Löw, R.; Hampel, F.; Stachel, H.-D.; Lentmaier, J.; Peters, K.; Peters, E.-M.; von Schnering, H. G. *Angew. Chem., Int. Ed. Engl.* **1995**, *34*, 993−995. (e) Mann, S.; Huttner, G.; Zsolnai, L.; Heinze, K. *Angew. Chem., Int. Ed. Engl.* **1996**, *35*, 2808−2809. (f) Enemark, E. J.; Stack, T. D. P. *Angew. Chem., Int. Ed.* **1998**, *37*, 932. (g) Amoroso, A. J.; Jeffery, J. C.; Jones, P. L.; McCleverty, J. A.; Thorton, P.; Ward, M. D. *Angew. Chem., Int. Ed. Engl.* **1995**, *34*, 4, 1443−1446.

(18) Corey, E. J.; Cheng, X.-M. *The Logic of Chemical Synthesis*; John Wiley & Sons: New York, 1989.

(19) (a) Stang, P. J.; Olenyuk, B. *Acc. Chem. Res.* **1997**, *30*, 502−518. (b) Fujita, M.; Yu, S.-Y.; Kusukawa, T.; Funaki, H.; Ogura, K.; Yamaguchi, K. *Angew. Chem., Int. Ed.* **1998**, *37*, 2082−2085. (c) Fujita, M.; Sasaki, O.; Mitsuhashi, T.; Fujita, T.; Yazaki, J.; Yamaguchi, K.; Ogura, K. *Chem. Commun.* **1996**, 1535−1536.

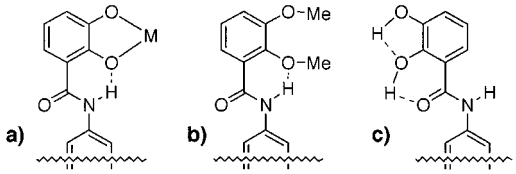

Figure 2. When coordinated to a metal (a), the catecholamide binding unit has a rigidly fixed geometry as a result of the hydrogen bond between the amide proton and the *ortho*-oxygen. This hydrogen bonding motif is preserved in the methyl-protected ligand (b), but reversed in the unmetalated, free ligand (c).

the onset of the reaction. Consequently, the metal−ligand bonds must be labile enough to allow the initially formed kinetic products to rearrange into the thermodynamic product. This requirement precludes, on one hand, the use of kinetically inert metals such as Cr^{III} and Co^{III} as building blocks, and, on the other hand, the use of kinetically disfavored metal chelators such as rigid tetradentate ligands such as the pyrrolic nitrogens in porphyrins. This requirement also suggests that the reaction conditions need to be chosen so as to facilitate the rearrangement of kinetic products to the thermodynamic product, that is, by lowering the pH of the solution or using higher reaction temperatures.

Choice of a Suitable Ligand−Backbone Combination. The geometry of a particular ligand and its known interaction with a metal ion (see below) should contain all of the information required for the successful self-assembly of the desired cluster. This mandates a predetermined conformation of the ligand. Thus, the orientation of multiple binding units within a ligand must be either rigidly fixed or at least somewhat conformationally restricted.

With respect to the above considerations, the catecholamide binding unit (Figure 2) is a good choice for use in cluster formations because of the high thermodynamic stability, yet kinetic lability, when coordinated to trivalent metal ions, such as Fe^{III}, Ga^{III}, and Al^{III}, in an octahedral coordination environment.[20−23] The catecholamide functionality is a rigid binding unit as a result of a strong hydrogen bond between the amide hydrogen and the coordinating *o*-hydroxy oxygen (Figure 2a). This hydrogen bond imposes a coplanar arrangement of the amide with the catecholate unit, reducing the degrees of freedom in the ligand and making the conformation of the coordinated ligand calculable.

Due to the electronically preferred coplanarity of the amide functionality with aromatic systems, any combination of the catecholamide moieties with an aromatic backbone (e.g., a benzene or naphthalene backbone) produces a rigid oligobidentate ligand system that predisposes the coordinating groups in a highly predictable way. The crystal structure of the methyl-protected ligand Me_6**A** illustrates these features. The methyl-protected catecholamides show the same H-bond pattern as the metalated catechol amides (Figure 2b). In contrast, the conformation of the catechol moiety of the unprotected ligand is generally 180° rotated, the hydroxy functionality in the 2-position forming one H-bond to the amide oxygen and the hydrogen

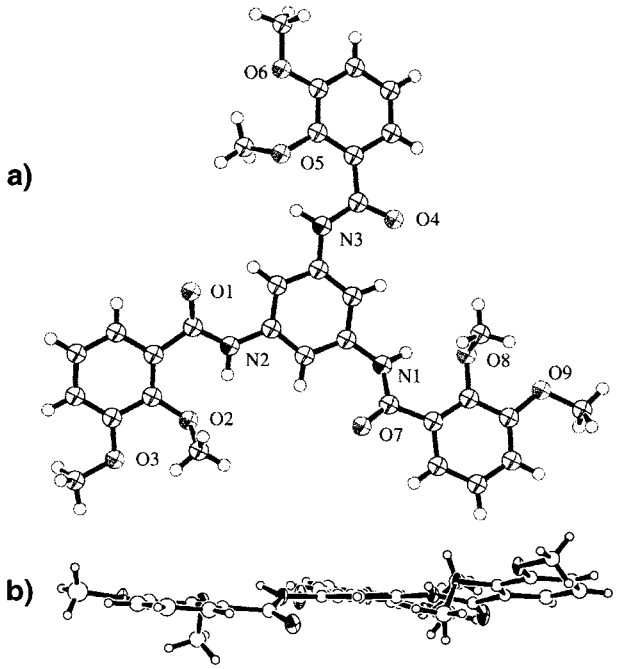

Figure 3. ORTEP diagram of Me_6**A** illustrating (a) the molecular three-fold symmetry of the ligand and (b) its planar configuration.

of the hydroxy functionality in the 3-position being shared between both hydroxy groups (Figure 2c). The compound Me_6**A** crystallizes in the space group $P2_1/a$ with approximate three-fold symmetry (Figure 3a). The H-bonds between the amide nitrogen and the catechol oxygen are clearly expressed. Also, as anticipated, the three catecholamide functionalities are, albeit to different degrees, predominantly coplanar to the central ring (Figure 3b).

Thermodynamic Implications of Ligand Rigidity. An example best illustrates the effect of ligand rigidity on the thermodynamics controlling complex formation. Consider the formation of an M_2L_3 helicate formed by a ligand (L) with two (bidentate) binding sites and a metal (M) with three acceptor sites (i.e., for three bidentate ligands forming a pseudooctahedral coordination sphere). The only M:L ratio that can satisfy the binding requirements of both the ligand and metal components of the cluster is 2M:3L. Now consider an equilibrium between two triple helicates of the stoichiometry M_2L_3 and its dimer, a tetrahedron of the stoichiometry M_4L_6:

$$2\ M_2L_3 = M_4L_6$$

$$K_{eq} = [M_4L_6]/[M_2L_3]^2 \cong 1$$

Assuming a ligand system that has no unfavorable steric constraints and in which the M−L interactions are the sole driving forces for cluster formation, both geometries are equally possible, and the equilibrium constant should be approximately unity. If the initial concentration of the M_2L_3 triple helicate is 2 mM, then the concentration of the M_4L_6 tetrahedron will only be 4 μM! This example illustrates the widely recognized principle in supramolecular self-assembly: that entropy will favor the largest number of particles with the smallest possible stoichiometry. How, then, does one enforce the formation of assemblies with stoichiometries which are *multiples* of the empirical ratio of ligands to metals? Specifically, how does one expand selectively an M_1L_1 complex to an M_4L_4 cluster or, likewise, an M_2L_3 helicate to an M_4L_6 tetrahedron? The answer lies in the geometric constraints that must be incorporated into

(20) Borgias, B. A.; Barclay, S. J.; Raymond, K. N. *J. Coord. Chem.* **1986**, *15*, 109−123.
(21) (a) Caudle, M. T.; Crumbliss, A. L. *Inorg. Chem.* **1994**, *33*, 4077−4085. (b) Borgias, B.; Hugi, A. D.; Raymond, K. N. *Inorg. Chem.* **1989**, *28*, 3538−3545.
(22) (a) Garrett, T. M.; Miller, P. W.; Raymond, K. N. *Inorg. Chem.* **1989**, *28*, 128−133. (b) Kappel, M. J.; Pecoraro, V. L.; Raymond, K. N. *Inorg. Chem.* **1985**, *24*, 2447−2452.
(23) Karpishin, T. B.; Stack, T. D. P.; Raymond, K. N. *J. Am. Chem. Soc.* **1993**, *115*, 6115−6125.

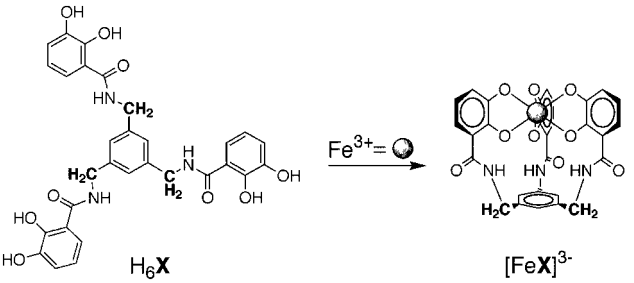

Figure 4. As shown in the enterobactin analogue H_6**X**, simple addition of a methylene group between the three-fold benzene scaffold and the catecholamide binding units gives the ligand enough flexibility to allow each of the arms to coordinate a single metal ion. This type of ligand flexibility must be avoided if multimetal clusters are desired.

the ligand design, prohibiting the formation of lower-order structures. This feat can be accomplished by making the ligand too rigid for more than one chelation site to simultaneously bind the same metal.

The ligand H_6**A** when compared to the structurally similar enterobactin model compound H_6**X** exemplifies this effect of rigidity (Figure 4). H_6**X** differs from H_6**A** only by the presence of the methylene groups between the phenyl backbone and the three ligand arms. This introduction of flexibility into the ligand allows all three catecholate moieties to chelate to one metal simultaneously. Even though the flexible ligand could easily adopt conformations to accommodate higher-order complexes of the stoichiometry M_n**X**$_n$, because the smallest combination is favored, only the M_1**X**$_1$ monomer can be detected. Removal of the methylene groups results in ligand H_6**A**. This ligand is unable to coordinate a single metal ion with more than one catechol group; as a result, attaining a coordinatively saturated M_1L_1 stoichiometry is impossible. The alternative higher-order M_4L_4 structure that this ligand is forced to form will be described below.

Definition of Terms. To describe our approach to the rational design of supramolecular clusters, it is useful to define terms that more accurately describe the relevant geometric relationships between the metal coordination spheres and the ligands. The vector that represents the interaction between a ligand and metal is the *Coordinate Vector* (Figure 5a). In the case of a monodentate ligand, this vector is simply the one directed from the coordinating atom (or electron pair) of the ligand toward the metal ion. In the case of a bidentate ligand, this vector bisects the bidentate chelating group and is directed toward the metal ion.

When using chelating ligands, the plane orthogonal to the major symmetry axis of a metal complex is the *Chelate Plane* (Figure 5b); all of the coordinate vectors of the chelating ligands lie in the chelate plane. In an octahedral to trigonal prismatic coordination geometry, three bidentate ligands generate a three-fold axis at the metal center. While the geometry of such a complex is often described by the twist angle,[24] here it is convenient to describe this geometry with respect to the orientation of each bidentate ligand.

The *Approach Angle* is defined as the angle between the axis determined by the two donor atoms and the three-fold axis of the (pseudo)octahedron. This angle is expressed by the vector relationship described in Figure 6. An approach angle of 0° corresponds to a trigonal prism, while an approach angle of 35.3° corresponds to that of a perfect octahedral complex. Tris(catecholate) complexes of Fe^{III}, for example, tend to be distorted toward trigonal prismatic geometry, having an approach angle near 23° (40° twist angle).[20]

(24) Cotton, F. A.; Wilkinson, G.; Murillo, C. A.; Bochmann, M. *Advanced Inorganic Chemistry*, 6th ed.; John Wiley: New York, 1999.

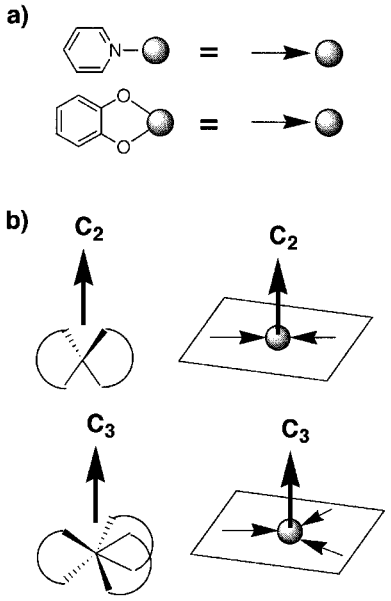

Figure 5. Illustrations of (a) *Coordinate Vectors* and (b) *Chelate Planes.*

Design of the Tetrahedral Clusters. Design Strategy for a Tetrahedral M_4L_4 Cluster. A tetrahedral cluster of the stoichiometry M_4L_4 can be described as four metal ions in a tetrahedral array connected by four three-fold symmetric ligands: Each ligand acts as one face of a tetrahedron, while each metal ion acts as a vertex of the tetrahedron. Since a tetrahedron has three-fold symmetry through each vertex, the metal−ligand junction must also be able to achieve three-fold symmetry. One way this can be accomplished is by using a metal ion that prefers an (pseudo)octahedral geometry. Since each of the metal ions has six acceptor sites and the metal-to-ligand ratio is 1:1, then each ligand must have six donor sites. With these stoichiometric and geometric considerations in mind, the problem of designing a tetrahedral supramolecular assembly of the stoichiometry M_4L_4 can be reduced to designing a rigid three-fold symmetric ligand that positions its three coordinate vectors correctly. This analysis can best be accomplished by determining the ideal approach angle for a cluster of this type.

A schematic representation of a tetrahedral M_4L_4 cluster in which the faces of the tetrahedron are made up of strictly planar three-fold symmetric ligands (represented by the large yellow faces) and the vertices are made up of (pseudo)octahedrally coordinated metal atoms (represented by the small red triangular faces) is depicted in Figure 7. The small red faces actually represent the previously described chelate planes, which are perpendicular to the three-fold axis at each metal vertex. In this design, the coordinate vector of each catecholate unit must lie simultaneously in both the ligand plane (yellow face) and the chelate plane (red face) at the metal vertex. The angle between a three-fold axis and the associated faces in a tetrahedron is 19.4°. If the bound ligands are planar and coordinate as shown, this angle corresponds to the approach angle. The experimentally obtained approach angles for mononuclear tris(catecholates) are ∼23°.[25,26] This, in turn, implies that the planar ligand to be used in the formation of a tetrahedral cluster is required to distort only a few degrees from planarity to comply with the ideal approach angle at the metal centers.

Design Strategies for the Synthesis of M_4L_6 Tetrahedral Clusters. Similar to the aforementioned M_4L_4 tetrahedral cluster,

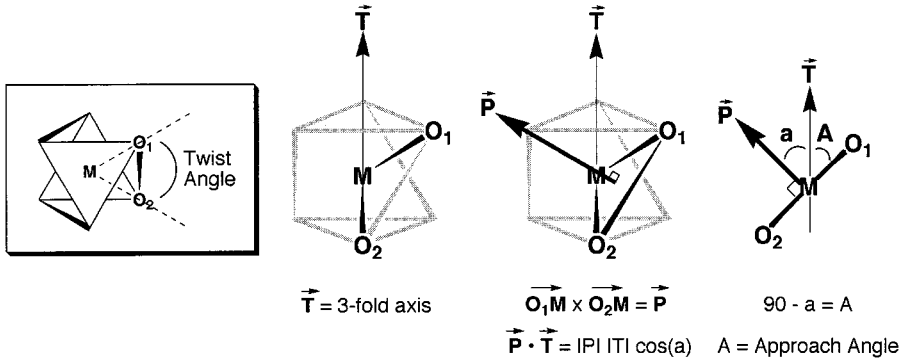

Figure 6. When designing high-symmetry clusters it is often useful to consider the *Approach Angle* of a chelating ligand around a metal center, rather than the twist angle. The approach angle can more easily be compared to the angles generated by a given cluster.

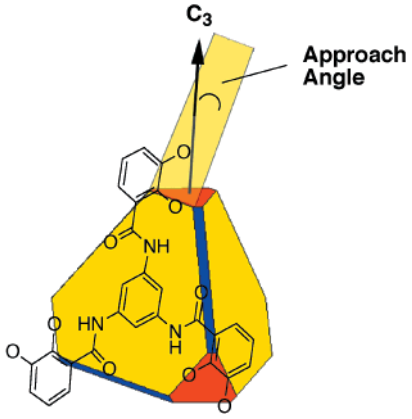

Figure 7. In this M_4L_4 design, the ligand H_6**A** will act as the face of the tetrahedron. The angle at which the extended three-fold plane crosses an adjacent three-fold axis is analogous to the approach angle of the ligand arm with the metal located at the tetrahedron vertex.

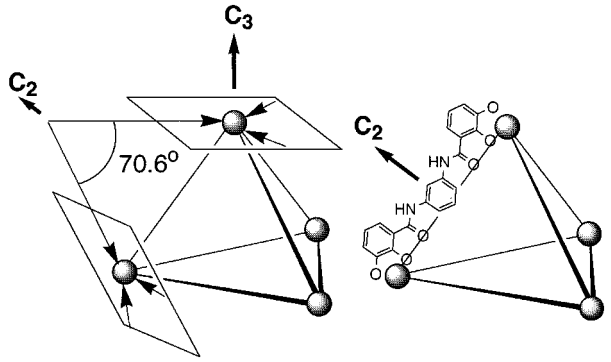

Figure 8. In this "Edge-On" M_4L_6 design, the ligand H_4**B** will act as one of the edges of the tetrahedron with the two-fold axis of the cluster being coplanar with the ligand. In this design, the angle between the coordinate vectors of the two-fold ligand is the primary consideration.

a tetrahedral cluster of stoichiometry M_4L_6 has four metal ions at the four vertices of a tetrahedron. In contrast, however, these four metal ions are linked by six two-fold symmetric ligands, each ligand acting as one of the six edges of the tetrahedron. Again, the interaction between a metal ion and the three ligands converging at each corner of the tetrahedron generates a three-fold axis through the formation of an (pseudo)octahedral coordination sphere around the metal. The smallest assembly that could result from the simultaneous satisfaction of the two- and three-fold symmetry requirements is an M_2L_3 complex. To avoid the entropically favored smaller cluster, geometric constraints must be incorporated into the rigid ligand design. We have described two different approaches to the rational design of such clusters.[27,28] Both approaches employ an ideally planar C_2-symmetric bis(bidentate) ligand with a rigid backbone, but the orientation of the C_2 axis of the cluster with respect to the mean plane of the ligand differs.

In the first design strategy, which we call the "Edge On" approach, the two-fold axis of the tetrahedron is coplanar with the plane defined by the ligand (Figure 8).[27] Since the coordinate vectors must lie within the chelate planes at each of the four metal vertices, the angle between the coordinate vectors within a given ligand must be 70.6°. (This angle is the supplement of 109.4°, the angle between the three-fold axes in a tetrahedron.) A 60° angle is formed between the chelate vectors for ligand H_4**B**; thus, the targeted tetrahedral structure can be achieved with only slight out-of-plane twisting by each of the chelating groups. The 60° angle between the coordinate vectors of ligand H_4**B** is the geometric implement enforcing the formation of the M_4L_6 assembly, since an M_2L_3 helicate would require that the coordinate vectors be parallel.[29,30]

An alternative design strategy for an M_4L_6 tetrahedron can be envisioned in which the two-fold axis of the tetrahedron is perpendicular to the plane of the ligand. This type of design strategy we will call the "Face On" approach (Figure 9).[31] If the ligand conformation is strictly planar, then the approach angle is 35.3°, identical to that of a perfect octahedral metal complex (equivalent to a twist angle of 60°). Mononuclear tris(catecholamide) complexes of Ga^{III} and Fe^{III} are known to be slightly distorted toward a trigonal prismatic coordination geometry (ca. 40° twist angle or 23° approach angle). Thus, slight out-of-plane twists of the ligands would be required to ideally accommodate these metals. Slight rotation of the catechol amide moiety along the backbone−amide axis can be envisioned to accomplish the required deviation.

The selectivity in the ligand H_4**C** for the formation of an M_4L_6 cluster versus a M_2L_3 helix is achieved using a naphthalene spacer, which causes the two catechol binding units to be offset from one another when the ligand is in the conformation

(25) (a) Borgias, B. A.; Cooper, S. R.; Koh, Y. B.; Raymond, K. N. *Inorg. Chem.* **1984**, *23*, 1009−1016. (b) Holmes, R. R.; Shafieezad, S.; Chandrasekhar, V.; Sau, A. C.; Holmes, J. M.; Day, R. O. *J. Am. Chem. Soc.* **1988**, *110*, 1168−1174.

(26) Albrecht, M.; Kotila, S. *Chem. Commun.* **1996**, 2309−2310.

(27) Beissel, T.; Powers, R. E.; Raymond, K. N. *Angew. Chem., Int. Ed. Engl.* **1996**, *35*, 1084−1086.

(28) Caulder, D. L.; Powers, R. E.; Parac, T.; Raymond, K. N. *Angew. Chem., Int. Ed.* **1998**, *37*, 1840−1843.

(29) Meyer, M.; Kersting, B.; Powers, R. E.; Raymond, K. N. *Inorg. Chem.* **1997**, *36*, 5179−5191.

(30) Powers, R. E. The Rational Design of Supramolecular Assemblies. Ph.D. Thesis, University of California, Berkeley, December 1997.

(31) Note that the M_4L_4 tetrahedron described earlier is also a "Face On" design.

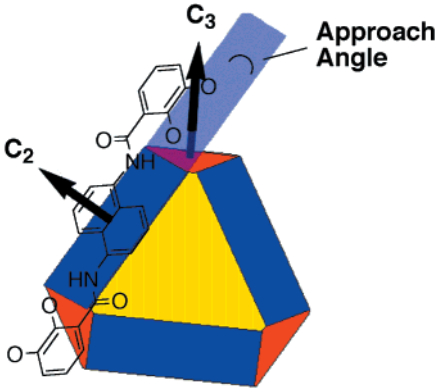

Figure 9. In this "Face-On" M_4L_6 design, the two-fold axis of the cluster is perpendicular to the ligand plane. In this design, the approach angle is the primary consideration.

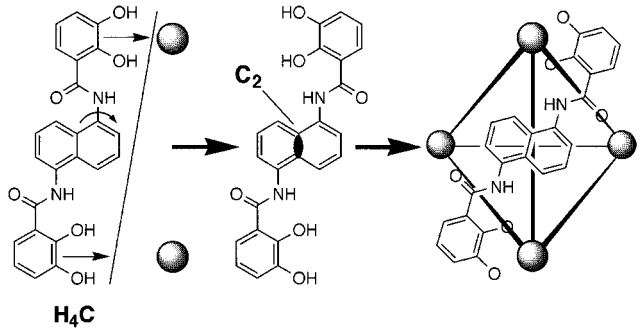

Figure 10. Ligand H_4**C** is deterred from forming an M_2L_3 cluster because of the offset of the chelating units created by the use of the naphthalene scaffold. Rotation around the arene−N bond puts the ligand in the conformation required to form an M_4L_6 tetrahedral cluster.

required for helicate formation, thus disfavoring the formation of a helicate (Figure 10).

Molecular Modeling. Prior to the actual ligand synthesis, the feasibility of the proposed metal−ligand systems is explored using molecular mechanics calculations.[32] Although these calculations do not guarantee that the proposed structure will form, they help eliminate structures that are nonviable due to unfavorable inter- and intraligand steric interactions. When comparing results of the molecular modeling calculations with actual crystal structures, it becomes evident that while the gross structure can be predicted fairly accurately, effects of hosts inside the clusters (or the absence of guests) cannot be predicted. Nor can it be predicted that certain clusters require a guest to be formed.[33] Nevertheless, we find molecular modeling to be an indispensable tool in the design of the clusters presented here.

Results and Discussion

Ligand Syntheses. All ligands used in this study belong to the same class of bis- and tris(catecholamides). They all were synthesized following established routes (Scheme 1). Polyamines **1**, **2**, or **3**, either commercially available or synthesized by reduction of the corresponding commercially available nitro compounds, were reacted with the acid chloride of 2,3-dimethoxybenzoic acid (**4**) under standard amide bond-forming conditions (excess Et_3N in CH_2Cl_2).[34] The resulting *O*-methyl-substituted ligands Me_6**A**, Me_4**B**, and Me_4**C** were deprotected

Scheme 1. Synthesis of Ligands H_6**A**, H_4**B**, and H_4**C** Used in This Study

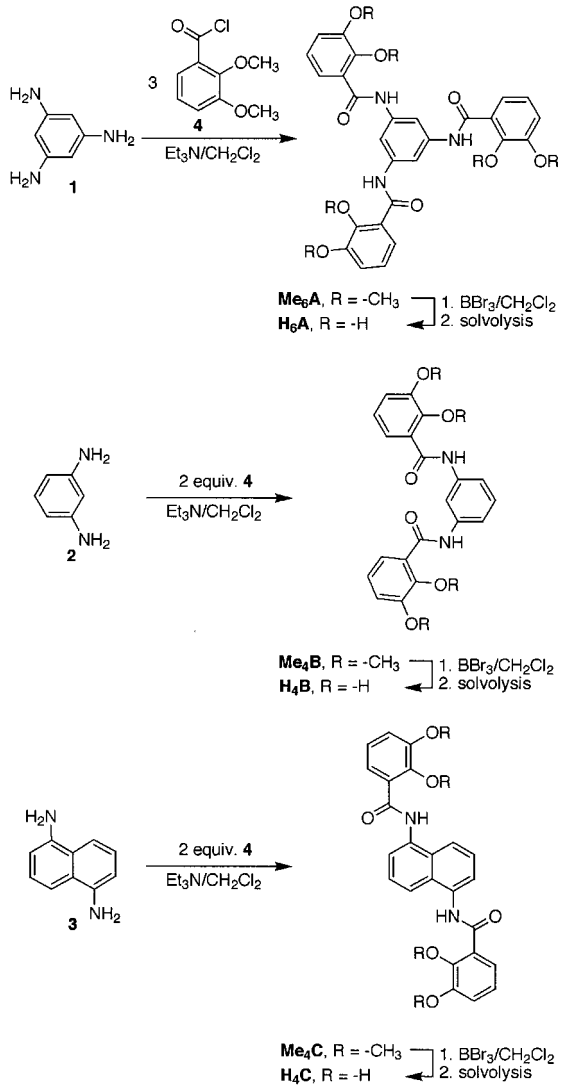

by reaction with BBr_3 to produce, in generally excellent overall yields, the polycatecholamide ligands H_6**A**, H_4**B**, and H_4**C**, respectively.

This scheme for the synthesis of catecholamide oligobidentate ligands is most versatile.[26,35] The scheme is limited only by the availability of the amine backbone and the resistance of the resulting amide to the deprotection conditions. For acid-sensitive backbones, however, the use of the benzyl-protected 2,3-hydroxybenzoic acid chloride, and subsequent removal of the protecting groups under reductive conditions, has been shown to be feasible.[36]

Synthesis of M_4A_4 Clusters. Ligand H_6**A** reacts with stoichiometric amounts of $Ga(acac)_3$ under basic conditions (3 equiv of KOH) in MeOH to give a precipitate whose ^{1}H NMR (300 MHz, D_2O) indicates the formation of one defined and highly symmetric species (see also below). The mass spectrum (ESI, cation detection) of the Ga^{III} complex, as its K^+ salt, shows

(32) *CAChe* MM2 Force Field, V4.0; Oxford Molecular Group, Inc.: U.S.A., 1997.

(33) For instances in which the cluster formed only in the presence of a guest see, e.g.: refs 14b and 26; for instances in which the cluster conformation was affected by a guest, see: Xu, J. D.; Parac, T. N.; Raymond, K. N. *Angew. Chem., Int. Ed.* **1999**, *38*, 2878−2882.

(34) Weitl, F. L.; Raymond, K. N. *J. Am. Chem. Soc.* **1980**, *102*, 2289−2293.

(35) (a) Enemark, E. J.; Stack, T. D. P. *Angew. Chem., Int. Ed. Engl.* **1995**, *34*, 996−998. (b) Enemark, E. J.; Stack, T. D. P. *Angew. Chem., Int. Ed.* **1998**, *37*, 932−935. (c) Albrecht, M. *Chem. Eur. J.* **1997**, *3*, 1466−1471. (d) Albrecht, M.; Riether, C. *Synthesis* **1997**, 957. (e) Albrecht, M. *Synlett* **1996**, 565.

(36) Schuda, P. F.; Botti, C. M.; Venuti, M. C. *OPPI Briefs* **1984**, *16*, 119−123.

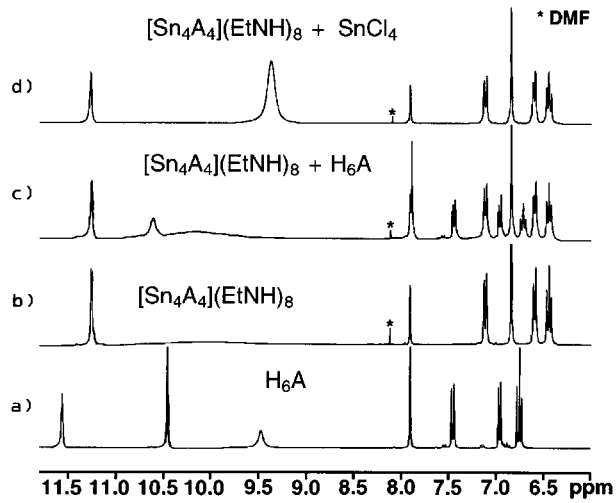

Figure 11. ^{1}H NMR (400 MHz, 25 °C, DMSO-d_6) of the ligand $\mathbf{H_6A}$ (a) and the complex $[Sn_4\mathbf{A}_4]^{8-}$ (b). Neither excess ligand (c) nor excess $SnCl_4$ (d) disrupts the formation of the $[Sn_4\mathbf{A}_4]^{8-}$ tetrahedral cluster.

two major peaks at *m*/*z* 1463.4 and 988.6. Under these low-resolution conditions, the first peak can be assigned to the species $\{[Ga_4\mathbf{A}_4]^{12-}\cdot 14K^+\}^{2+}$ or $\{[Ga_2\mathbf{A}_2]^{6-}\cdot 7K^+\}^{+}$ and is, therefore, not unambiguously indicative of the formation of a tetrahedron. The peak at *m*/*z* 988, however, attributed to the trication $\{[Ga_4\mathbf{A}_4]^{12-}\cdot 15K^+\}^{3+}$ provides an indication for the formation of the desired cluster since it cannot be rationalized by a metal:ligand stoichiometry lower than 4:4; thus, this evidence strongly suggests the formation of the tetrahedron.

Despite these encouraging results, we were unsuccessful at growing crystals suitable for analysis by X-ray diffraction. Presumably the −12 charge of these tetrahedra and their good solubility in MeOH, H_2O, DMSO, and DMF forestalled the formation of high-quality single crystals.

The overall charge of the cluster can be reduced by using higher-oxidation state metals; for instance, M^{IV} metal ions will reduce the charge from −12 to −8. Pseudooctahedral tris(catecholate) complexes of V^{IV}, Sn^{IV}, and Ti^{IV}, for example, are known. While the formation of the V^{IV} tris(catecholate) species is most sensitive to the particular conditions chosen,[37] the opposite can be said for the formation of the Sn^{IV} and Ti^{IV} species.[25] For these reasons we chose to investigate the use of Sn^{IV} and Ti^{IV} in the construction of these self-assembled clusters.

A DMF solution of 1 equiv of $H_6\mathbf{A}$ combined with 1 equiv of $SnCl_4$ and an excess of Et_3N, heated under reflux for 12 h, produces a clear and colorless solution which, when evaporated to dryness under vacuum, results in the formation of a pale pink microcrystalline solid of the composition $[Sn_4\mathbf{A}_4](Et_3NH)_8\cdot x Et_3NHCl$ ($x = 3-4$). Attempts to remove the excess triethylammonium chloride by recrystallization of the salt mixture from a variety of solvents failed to produce a triethylammonium-free product. The ^{1}H NMR (300 MHz, DMSO-d_6) spectrum indicated the formation of only one defined species in which the ligand is located in a three-fold symmetric environment (Figure 11b). The proton signals for the hydroxy groups of the ligand (Figure 11a) disappeared, and all other signals shifted in a way consistent with complex formation. In particular, the NH proton shifted downfield as expected due to the H-bond produced upon complexation. Addition of an aliquot of excess ligand did not cause any shift or line-broadening of the peaks of the metal complex (Figure 11c), even at temperatures up to 100 °C. Likewise, the addition of 1 equiv of excess $SnCl_4$ to the cluster dissolved in DMF does not affect the spectrum (Figure 11d). These experiments demonstrate that the single set of resonances observed in the ^{1}H NMR spectrum are not a result of a rapidly exchanging polymeric system, but rather they are attributable to a discrete metal−ligand species. It seems reasonable to predict that pronounced cooperativity effects prevent fast ligand-exchange processes in these types of tethered clusters. The electrospray mass spectrum of the $[Sn_4\mathbf{A}_4]^{8-}$ complex further provided data to prove the formation of the desired M_4L_4 tetrahedron (see below).

The analogous Ti^{IV} complex $[Ti_4\mathbf{A}_4](Et_3NH)_8$ was prepared by a modified procedure. A solution of $Ti(O\textit{n}\text{-}Bu)_4$ in MeOH was combined with $H_6\mathbf{A}$ in MeOH/excess Et_3N. The solution quickly turned orange and, after 12 h, a gelatinous orange precipitate formed. The ^{1}H NMR spectrum of a DMSO-d_6 extract of this precipitate taken at 25 °C shows the presence of a mixture of (polymeric) compounds. Heating of the sample to 120 °C results, over the course of several hours, in a partial simplification of the spectrum. This experiment provided the guide for the next step: dissolution of the centrifuged and washed precipitate in DMF under reflux for 12 h. This step facilitated the rearrangement of the kinetic product mixture into one thermodynamic product; ^{1}H NMR spectra of samples taken from this solution showed the presence of one major product characterized by a single set of sharp resonances. Gas-phase diffusion of MeOH into this DMF solution produced orange crystals of $[Ti_4\mathbf{A}_4](Et_3NH)_8$. The ^{1}H NMR spectrum of the crystals dissolved in DMSO-d_6 was very similar in appearance to those observed for the Ga^{III} and Sn^{IV} species, giving an indication of successful cluster formation. This finding was also supported by the electrospray mass spectrum of the complex (see below).

While this procedure produced crystals of analytical and single-crystal X-ray diffraction quality (see below), it also highlights the disadvantage of using the much less kinetically labile ion Ti^{IV}, as compared to Ga^{III} or Fe^{III}. The kinetic product is not the desired cluster and is removed from the metal−ligand equilibrium by precipitation. A rearrangement step at elevated temperature and in a polar donor solvent is required to produce the designed thermodynamic product. The use of bases other than Et_3N (i.e., NaOH, KOH, CsOH, morpholine, pyridine) did not produce the clusters cleanly, while the use of Me_4NOH produced the cluster with greatly reduced solubility in MeOH and DMSO. These observations provide some rationalization of the fact that in the solid (crystal structure) and gas phase (mass spectrum) this octaanionic cluster (and the clusters to be described below) shows a very strong association with its triethylammonium countercations. Evidently, these interactions provide additional driving force for the formation of the desired clusters in a crystalline state. The reaction of a variety of Ti^{IV} sources ($TiCl_4$ or freshly precipitated TiO_2) in hot or cold DMF did not produce the expected cluster in a clean fashion. Likewise, the clean formation of the Sn^{IV}-based cluster was not possible with the methodology detailed for the Ti^{IV}-based tetrahedron. We assume that the differences of the metals and metal sources with respect to Lewis acidity, rate of hydrolysis, etc. require individualized reaction conditions. It should be noted, however, that once formed the respective clusters could be detected by NMR and mass spectrometry under a wide range of reaction conditions, attesting to the high thermodynamic stability of the products; only their isolation and preparation by simple means required the individualized procedures.

Crystal Structure of $[Ti_4\mathbf{A}_4](Et_3N)_8$. Slow gas-phase diffusion of MeOH at room temperature into a DMF solution of

(37) Cooper, S. R.; Koh, Y. B.; Raymond, K. N. *J. Am. Chem. Soc.* **1982**, *104*, 5092−5102.

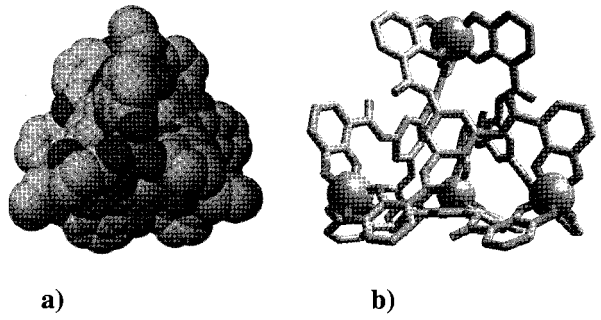

Figure 12. Based on the X-ray structure coordinates, $[Ti_4\mathbf{A}_4]^{8-}$ in both a space-filling (a) and wire-frame (b) representation.

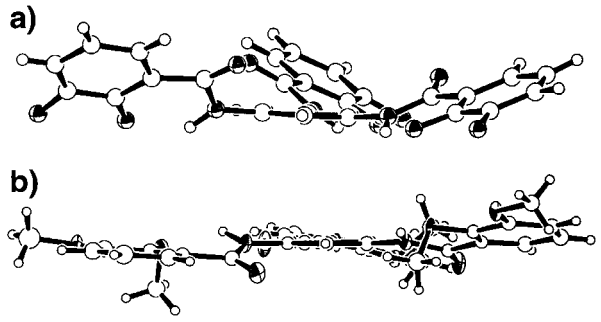

Figure 13. In the $[Ti_4\mathbf{A}_4]^{8-}$ cluster, the ligand is significantly distorted (a) from the planarity observed in the uncoordinated ligand (b).

$[Ti_4\mathbf{A}_4](Et_3NH)_8$ produced orange tablets of a quality suitable for analysis by X-ray diffraction. The single-crystal structure provided the ultimate proof of the proposed tetrahedral cluster.[38] Two views of the cluster in a space-filling and framework representation, respectively, are shown in Figure 12. The four three-fold symmetric ligands are required by our design to lie on the four faces of the $[Ti_4\mathbf{A}_4]^{8-}$ tetrahedron and are linked at the four tetrahedron vertices by the four metal ions. The compound crystallizes in space group $R\bar{3}c$ with 12 molecules in the unit cell. The cluster lies on a crystallographic three-fold axis but has molecular symmetry of the pure rotation group *T*, such that all metal ions within a given cluster have the same chirality (all Δ or all Λ). Hence, the compound crystallizes as a racemic mixture of homoconfigurational tetrahedra. The eight triethylammonium counterions are highly disordered, but the nitrogen atoms are clearly within hydrogen-bonding distance to either the carbonyl or the peripheral phenolate oxygens of the cluster. There is no evidence that the small cavity of the tetrahedron contains a guest (compare to the larger $[Fe_4\mathbf{C}_6]^{12-}$ cluster described below). Despite the hydrogen bonds between the amide proton and the phenolic oxygens, the catechol amides are more distorted from planarity than required by the design of the cluster. Figure 13a shows the side view of one ligand as it appears in the cluster. Compared to the side view of the uncomplexed ligand (Figure 13b), it becomes evident that this distortion can be attributed to the compulsion of the system to minimize the empty volume of the cavity. This may also be the reason for the larger than expected (19.4°) approach angle of 28°.

It should be noted that this is not the first tetrahedral cluster with stoichiometry M_4L_4; a related cluster has appeared in the literature.[39] Although the formation of this cluster was reported as serendipitous, its structure and formation highlight the building principles exemplified here. In particular, the fact that the ligand used in these studies was flexible and, depending on the size of the metal used, formed M_1L_1 or M_4L_4 complexes demonstrates the importance of incorporating rigidity into the ligand design. And as detailed above, our design does not allow the formation of an ML species. [A tetrahedral Tl_4L_4 cluster in which a tetrahedral M−M bond containing tetrahedral arrangement of four Tl^+ ions is capped by four ligands is only related by stoichiometry and not connectivity.[40]]

Synthesis of $M_4\mathbf{B}_6$ Clusters. The synthesis and characterization of an M_4L_6 tetrahedral cluster based on the "Edge On" design (see Figure 8) has been previously reported using a bis(hydroxamate) ligand.[29,40] A catecholate version based on ligand $H_4\mathbf{B}$ is described here. Reaction of 6 equiv of $H_4\mathbf{B}$, 4 equiv of $Ga(acac)_3$, and 12 equiv of KOH in methanol led to the precipitation of a white microcrystalline product after six to 8 h. The solubility of the cluster is much lower in methanol than that of the analogous helicates,[29,41] but both are readily soluble in water. The ^1H NMR spectrum of the complex in D_2O shows only one set of peaks, indicating that the ligands in the complex are in symmetry-related environments and that the C_2 axis of the ligand is maintained. This type of spectrum could be interpreted as the averaged position of the peaks if the ligands are in rapid exchange. This possibility can be ruled out by examining the ^1H NMR spectrum of the cluster prepared in the presence of excess ligand. Analogous to the previously described experiments with complexes of $H_4\mathbf{A}$, the spectrum of the mixture shows two sets of peaks, one for the complex and one for the excess ligand. In this case, however, these results do not rule out the presence of an M_2L_3 cluster. If lone pair donation of the amide nitrogens into the aromatic backbone of $H_4\mathbf{B}$ is insufficient to disfavor large deviations from planarity, then the chelate groups could rotate around the N−arene bond to be perpendicular with the backbone. This conformation would allow for the correct arrangement of coordinate vectors and chelate planes for an M_2L_3 cluster.

In a low-resolution positive ion electrospray mass spectrum, strong signals are seen for the $\{[Ga_4\mathbf{B}_6]\cdot 14K\}^{2+}$ doubly charged, the $\{[Ga_4\mathbf{B}_6]\cdot 15K\}^{3+}$ triply charged, and the $\{[Ga_4\mathbf{B}_6]\cdot 16K\}^{4+}$ quadruply charged ions. Because the charge states of the peaks could not be verified, the doubly and quadruply charged ions might be assigned to the full and half mass peaks of a corresponding $\{[Ga_2\mathbf{B}_3]\cdot 7K\}^{2+}$ cluster. The triply charged ion, however, cannot be rationalized by the smaller M_2L_3 cluster and appears to be diagnostic in assigning the structure as a tetrahedron.

Synthesis of $M_4\mathbf{C}_6$ Clusters. Reaction of 6 equiv of $H_4\mathbf{C}$, 4 equiv of $Ga(acac)_3$, 12 equiv of KOH, and 12 equiv of Et_4NCl in methanol leads to a yellow precipitate which analyzes as $K_5(Et_4N)_7[Ga_4\mathbf{C}_6]\cdot 8H_2O$ that shows unusual features in the ^1H NMR spectrum (Figure 14).[27] A ratio of seven Et_4N^+ counterions to six ligands is observed, with the seven counterions being split into two sets in a ratio of 6:1. The larger set of Et_4N^+ peaks ($\delta = 2.49$, q; 0.72, t) is shifted slightly upfield from free Et_4NCl ($\delta = 3.26$, q; 1.27, t), while the smaller set is shifted *substantially* upfield, showing up at negative ppm ($\delta = -0.70$, m; -1.59, t)! The upfield shifts of the exterior Et_4N^+ resonances are attributed to a strong π−cation naphthalene and catechol rings of the ligands and the Et_4N^+ counterions (vide infra). On

(38) Brückner, C.; Powers, R. E.; Raymond, K. N. *Angew. Chem., Int. Ed.* **1998**, *37*, 1837−1839.

(39) Amoroso, A. J.; Jeffery, J. C.; Jones, P. L.; McCleverty, J. A.; Thornton, P.; Ward, M. D. *Angew. Chem., Int. Ed. Engl.* **1995**, *34*, 1443−1446.

(40) Rheingold, A. L.; Liable-Sands, L. M.; Trofimenco, S. *Chem. Commun.* **1997**, 1691−1692.

(41) Kersting, B.; Meyer, M.; Powers, R. E.; Raymond, K. N. *J. Am. Chem. Soc.* **1996**, *118*, 7221−7222.

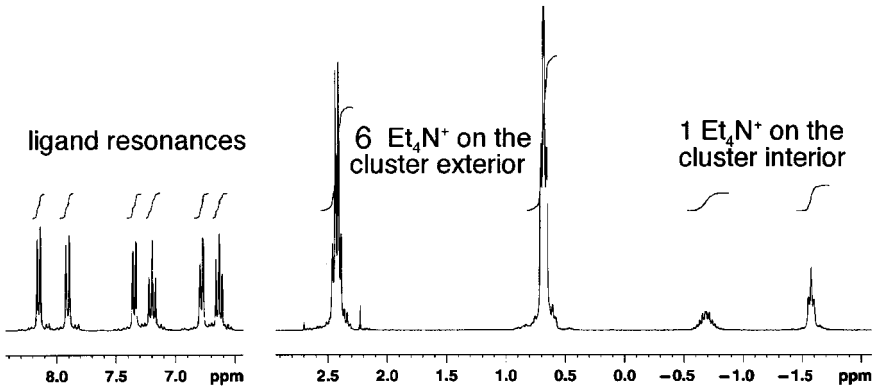

Figure 14. ^1H NMR (D_2O) of $K_5(Et_4N)_7[Ga_4\mathbf{C}_6]$ depicting the two sets of Et_4N^+ resonances characteristic of the exterior and encapsulated cations.

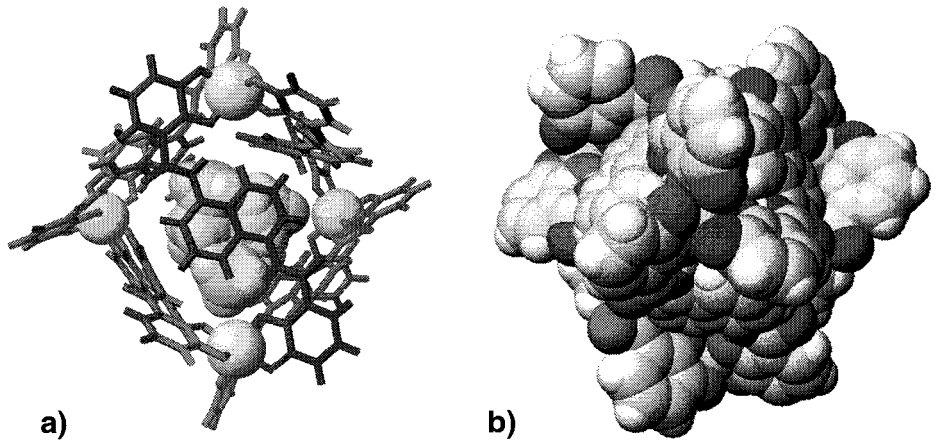

Figure 15. Based on the X-ray structure coordinates, $Et_4N^+\subset[Fe_4\mathbf{C}_6]^{12-}$ in both (a) wire-frame and (b) space-filling representations.

the basis of literature precedent this *extreme* upfield shift was taken as evidence of encapsulation of one of the Et_4N^+ counterions by the tetrahedral cluster.[42] Another interesting spectral feature of the encapsulated Et_4N^+ is that the CH_2 resonance is not a simple quartet, but rather it is a complex multiplet; the methylene protons are rendered diastereotopic inside the chiral host. This feature is an indication that the cluster is homoconfigurational (i.e., all Δ or all Λ coordination at the metal centers) giving rise to molecular symmetry of the pure rotation group *T* (racemic mixture of $\Delta\Delta\Delta\Delta$ and $\Lambda\Lambda\Lambda\Lambda$ clusters). It should be noted that computer modeling of the $M_4\mathbf{C}_6$ cluster correctly predicted that it would have *T* symmetry (all metal centers with the same chirality, all Δ or all Λ) and that there would be a substantial cavity inside the cluster. Computer models of the S_4 or C_3 symmetry isomers of the cluster were geometrically impossible.

Crystal Structure of $K_5(Et_4N)_7[Fe_4\mathbf{C}_6]$. The Fe^{III} analogue was prepared in a manner similar to that for the Ga^{III} complex. NMR studies of the Fe^{III} analogue were precluded by the paramagnetism of the Fe^{III} center. It was possible, however, to grow crystals of $K_5(Et_4N)_7[Fe_4\mathbf{C}_6]$ suitable for analysis by X-ray diffraction.[28] The cluster crystallizes with eight molecules of water and three molecules of methanol in the cubic space group $I\bar{4}3d$ (No. 220). One-third of the compound is crystallographically unique. The $[Fe_4\mathbf{C}_6]^{12-}$ anion lies on a crystallographic three-fold axis with *T* molecular symmetry; hence, the crystal is a racemic mixture of tetrahedra that have homoconfigurational (all Δ or all Λ) iron centers. As also observed in solution with the Ga^{III} complex, one of the Et_4N^+ counterions is located inside the cluster cavity (Figure 15a). The cluster is a tightly closed "box," with no aperture through the surface, as demonstrated by a space-filling model (Figure 15b).

The Fe−Fe distances in the cluster are, on average, 12.8 Å, bringing the overall size of the cluster just into the nanometer regime. The naphthalene rings are twisted along the arene−N bond, so that they bend into the cavity. The hydrogen bonds[23] between the amide proton and the coordinated catechol oxygen are still maintained, however. The angles between the least-squares planes calculated for the naphthalene backbone and the catechol rings are, respectively, 38.0° and 13.6° for one ligand and 20.7° and 65.3° for the other. We interpret this ligand distortion as a result of van der Waals interactions between the cluster and the encapsulated Et_4N^+. This van der Waals contact is clearly seen in Figure 16, which depicts a 2 Å thick slice through the center of the tetrahedral cluster. Solution studies (vide infra) suggest that this van der Waals contact is a result of more than just crystal-packing forces. There appears to be a strong π−cation interaction[43] between the aromatic rings of the ligands and the Et_4N^+ counterions.

The crystal packing of the $[Fe_4\mathbf{C}_6]^{12-}$ anion and the exterior Et_4N^+ cations is such that each dodecaanion is surrounded by six shared Et_4N^+ cations (Figure 17). Three of these Et_4N^+ cations are in close contact with the naphthalene rings of the ligand, and three are located in clefts between the catecholamide

(42) (a) Fujita, M.; Oguro, D.; Miyazawa, M.; Oka, H.; Yamaguchi, K.; Ogura, K. *Nature* **1995**, *378*, 469−471. (b) Jacopozzi, P.; Dalcanale, E. *Angew. Chem., Int. Ed. Engl.* **1997**, *36*, 613−615. (c) Mann, S.; Huttner, G.; Zsolnai, L.; Heinze, K. *Angew. Chem., Int. Ed. Engl.* **1996**, *35*, 2808−2809. (d) Parac, T.; Caulder, D. L.; Raymond, K. N. *J. Am. Chem. Soc.* **1998**, *120*, 8003−8004. (e) Fleming, J. S.; Mann, K. L. V.; Carraz, C.-A.; Psillakis, E.; Jeffery, J. C.; McCleverty, J. A.; Ward, M. D. *Angew. Chem., Int. Ed.* **1998**, *37*, 1279−1281. (f) Timmerman, P.; Verboom, W.; vanVeggel, F. C. J. M.; vanDuynhoven, J. P. M.; Reinhoudt, D. N. *Angew. Chem., Int. Ed. Engl.* **1994**, *33*, 2345−2348. (g) Bryant, J.; Blanda, M. T.; Vincenti, M.; Cram, D. J. *J. Am. Chem. Soc.* **1991**, *113*, 2167−2172.

(43) Ma, J. C.; Dougherty, D. A. *Chem. Rev.* **1997**, *97*, 1303−1324.

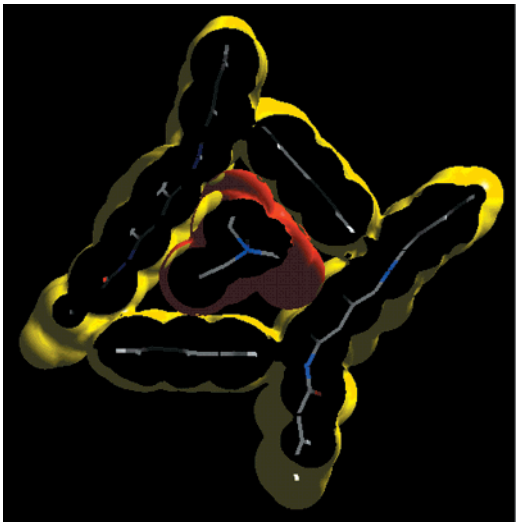

Figure 16. A 2 Å thick slice through the center of $Et_4N^+ \subset [Fe_4\mathbf{C}_6]^{12-}$ showing the surface contacts made between the ligands (yellow) and the encapsulated Et_4N^+ (red).

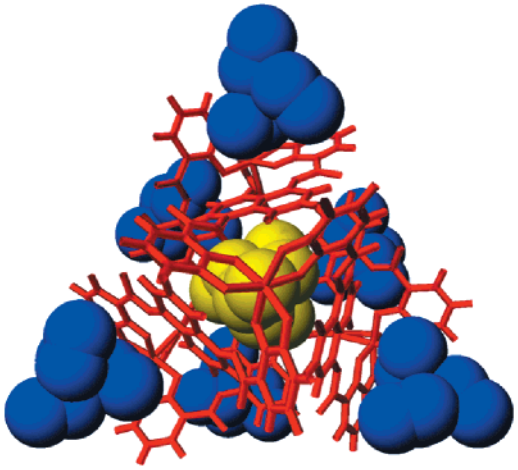

Figure 17. Six crystallographically identical Et_4N^+ cations (blue) surround the tetrahedral $[Fe_4\mathbf{C}_6]^{12-}$ cluster in the solid state. One Et_4N^+ cation (yellow) is encapsulated in the cluster interior.

rings. Because these cations are crystallographically identical, this Et_4N^+ must be surrounded by a naphthalene ring of one cluster and two catecholate rings of an adjacent cluster (Figure 18). The nitrogen atom of the exterior Et_4N^+ is located 4.0, 4.3, and 4.6 Å from the mean planes calculated for the two catecholamide moieties and the naphthalene ring, respectively. These distances are slightly shorter than the distances of the nitrogen atom of the encapsulated Et_4N^+ to the mean planes calculated for the two crystallographically independent naphthalene rings of the cluster (4.5 and 5.0 Å). This solid-state packing helps to explain why the cluster always precipitates as the $K_5(Et_4N)_7[M_4\mathbf{C}_6]$ salt ($M = Ga^{III}$, Fe^{III}) despite the fact that the reaction solution contains 12 equiv of both K^+ and Et_4N^+ cations. The upfield shifts of the proton resonances of the exterior Et_4N^+ cations compared to free Et_4N^+ are consistent with the idea that these contacts are maintained in solution. While the six exterior Et_4N^+ counterions prefer to be associated with the aromatic rings of the ligands, K^+ cations are preferentially coordinated by the catecholate oxygens at the corners of the tetrahedral cluster or by the carbonyl oxygens of the amide moieties on the ligands.

Host−Guest Chemistry Exhibited by $K_{11}(Et_4N)[Ga_4\mathbf{C}_6]$. To further investigate the interactions between the dodecaanionic tetrahedral cluster and the encapsulated and exterior Et_4N^+ cations, the titration of $K_{11}(Et_4N)[Ga_4\mathbf{C}_6]$ (D_2O, 300 MHz) with Et_4NCl was followed by ^1H NMR spectroscopy (Figure 19). The catechol resonances show little change, although they are shifted slightly upfield with increasing equivalents of Et_4N^+. The naphthalene resonances are shifted downfield, and protons of the encapsulated Et_4N^+ cations are shifted upfield. Initially, a linear change is observed, but a leveling off occurs after six to eight equivalents of Et_4N^+ per equivalent of $[Ga_4\mathbf{C}_6]^{12-}$ have been added. Similar inspection of the two ^1H resonances for the exterior Et_4N^+ cations reveals sigmoidal-shaped curves with inflection points near eight equivalents[44] of Et_4N^+ per equivalent of $[Ga_4\mathbf{C}_6]^{12-}$ (corresponding to one Et_4N^+ on the interior and six to seven Et_4N^+ on the exterior of the cluster). Thus, an apparent equivalence point, corresponding to one Et_4N^+ inside the cluster cavity and six to seven Et_4N^+ cations on the exterior of the cluster, is consistently indicated by all of the observed resonances.

These observations, along with the reproducible isolation of the cluster as the $K_5(Et_4N)_7[M_4\mathbf{C}_6]$ salt ($M = Ga^{III}$, Fe^{III}) and the packing of the exterior Et_4N^+ cations around the $[Fe_4\mathbf{C}_6]^{12-}$ anion in the crystal structure, attest to a well-defined superstructure of the Et_4N^+ cations and the $[M_4\mathbf{C}_6]^{12-}$ tetrahedral dodecaanion. The exterior of the tetrahedral cluster is surrounded by six Et_4N^+ cations, one Et_4N^+ per ligand in the cluster. This association might be explained in terms of a strong $\pi-$cation interaction between the aromatic rings of the ligands and the alkylammonium cations. It has been established that electrostatic interactions play a prominent role in prototypical $\pi-$cation interactions, and fundamental gas-phase studies have established the $\pi-$cation interaction to be among the strongest of noncovalent binding forces.[43]

An inspection of the CH_2 resonance of the encapsulated Et_4N^+ is also revealing (Figure 20). Initially, the CH_2 resonance of the encapsulated Et_4N^+ is a simple quartet. This feature in the ^1H NMR spectrum of $K_{11}(Et_4N)[Ga_4\mathbf{C}_6]$ contrasts with that in the spectrum of $K_5(Et_4N)_7[Ga_4\mathbf{C}_6]$, in which the methylene resonance is a complex multiplet. Addition of Et_4NCl to the solution of $K_{11}(Et_4N)[Ga_4\mathbf{C}_6]$ not only causes the proton resonances to shift, but it also causes the quartet to gradually split into a multiplet. Seemingly, in the absence of the adhering exterior Et_4N^+ cations, the cavity is large enough that the encapsulated Et_4N^+ does not "see" the chirality of the cluster host. The walls of the cluster are compressed, however, as the exterior Et_4N^+ cations adhere to the surface. The cavity then becomes smaller, and the encapsulated Et_4N^+ begins to experience the chiral environment of the *T* symmetry cluster host. These results imply that the cavity size is affected by the presence of Et_4N^+ cations on the cluster exterior.

A variable-temperature ^1H NMR spectroscopy experiment showed that the encapsulated Et_4N^+ and the exterior Et_4N^+ cations of $K_5(Et_4N)_7[Ga_4\mathbf{C}_6]$ do not coalesce up to 100 °C in D_2O. In fact, the peaks hardly shift. Inspection of the methylene resonance of the encapsulated Et_4N^+ reveals that heating does affect the interconversion of the diastereotopic protons, but even at 100 °C the protons are not equivalent (Figure 21).

Additional evidence for the solution structure of $K_5(Et_4N)_7[Ga_4\mathbf{C}_6]$ was obtained from 2D nuclear Overhauser effect spectroscopy (2D-NOESY).[45] Strong cross-peaks observed

(44) Second derivative plots of the shifts of the proton resonances for the exterior Et_4N^+ cations are both equal to zero at 8 equiv of Et_4N^+ per equivalent of $[Ga_4\mathbf{C}_6]^{12-}$. Note that the conditions for the experiments for Figures 21 and 22 differ slightly, hence the slight mismatch of overlap.

(45) Friebolin, H. *Basic One- and Two-Dimensional NMR Spectroscopy*, 2nd ed.; VCH: Weinheim, 1993.

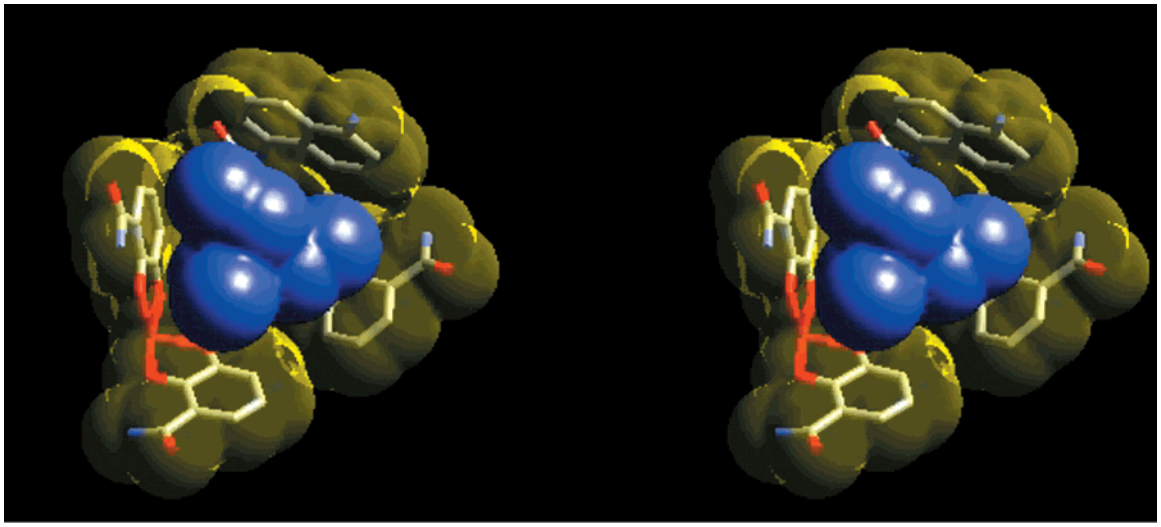

Figure 18. Stereoview of the environment of the exterior Et_4N^+ cation in the crystal structure of $K_5(Et_4N)_7[Fe_4C_6]$. The Et_4N^+ cation is surrounded by the aromatic naphthalene and catecholamide rings.

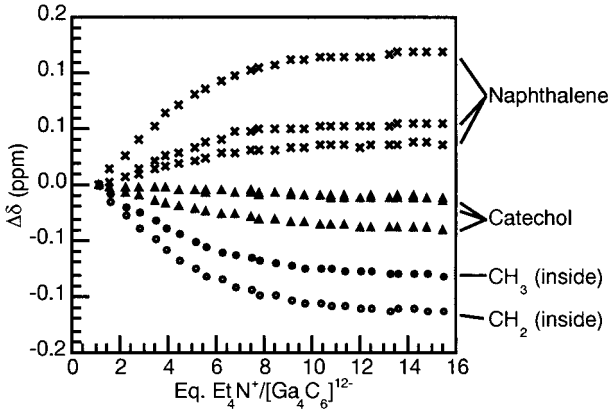

Figure 19. Shifts of the ^1H NMR resonances for the ligand (catechol and naphthalene rings) and the encapsulated Et_4N^+ countercation with increasing equivalents of Et_4NCl.

between the encapsulated Et_4N^+ and *only* the naphthalene resonances of the cluster are consistent with the encapsulation of one molecule of Et_4N^+ (Figure 22). Interestingly, cross-peaks are also observed between the six Et_4N^+ cations located on the exterior of the cluster and the naphthalene and catechol protons on the ligands of the tetrahedral cluster. This evidence indicating that the exterior Et_4N^+ cations also interact strongly with the aromatic sections of the cluster backbone is consistent with our findings from titration studies and the X-ray crystallographic results (vide supra).

The NOE changes the intensities of the observed signals as a result of dipole−dipole, or in effect through-space, relaxation of the nuclear spin. In small molecules with short rotational correlation times, t_c, one type of relaxation mechanism dominates, which has the effect of amplifying the NOE signal. In large molecules with long rotational correlation times, a second type of relaxation mechanism dominates that has the effect of decreasing the NOE signal.[45] Due to the large size of the cluster the majority of NOE peaks were found to be negative, indicating that the cluster is in the slow-tumbling regime. The encapsulated Et_4N^+ is the only positive NOE peak observed, implying that it is tumbling inside the cluster cavity in the fast-tumbling regime independent of the slower-tumbling host cluster.

Cross-peaks were also observed between the encapsulated and exterior Et_4N^+ cations. This observation suggested that the inner and outer Et_4N^+ molecules are exchanging on the NMR

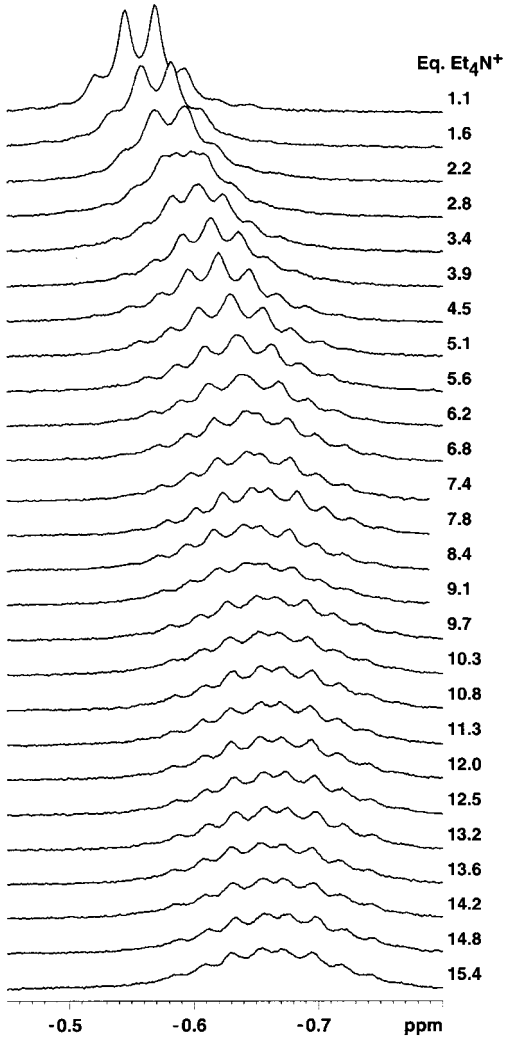

Figure 20. The methylene resonance of the encapsulated Et_4N^+ gradually changes from a quartet to a multiplet as Et_4NCl is added to a solution of $K_{11}[Et_4N][Ga_4C_6]$.

time scale. While typical line-shape analysis of 1D NMR spectra is applicable to the study of processes occurring with rate constants between 1 and 10^4 s^{-1}, the saturation transfer technique (NOESY and EXSY) is applicable to slower processes with rate

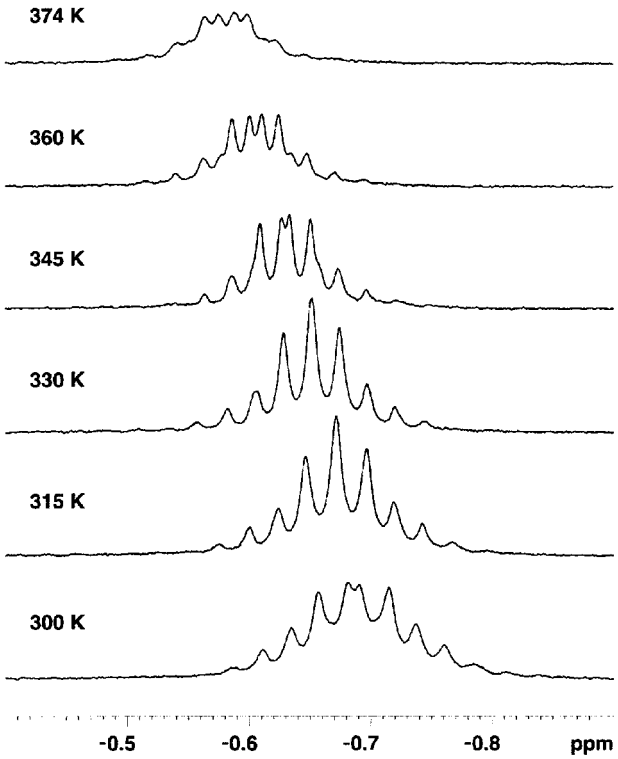

Figure 21. Heating a solution of $K_5[Et_4N]_7[Ga_4\mathbf{C}_6]$ up to 100 °C does not cause the diasterotopic methylene protons to become equivalent.

constants on the order of 10^{-1} to 10^2 s^{-1}.[46] To confirm that these cross-peaks were indeed indicative of an exchange process, 2D exchange spectroscopy (EXSY) was employed. In the 2D-EXSY experiment, which is similar to the 2D-NOESY experiment, the cross-peaks provide a clear picture of the exchange process.[46] 2D-EXSY spectra were recorded at different mixing times, τ_m. When the mixing time was increased from 0.75 to 1.5 s, the intensity of the cross-peaks increased approximately two-fold.

Since the crystal structure of $K_5(Et_4N)_7[Fe_4\mathbf{C}_6]$ has shown that the cluster is a tightly closed box lacking holes on the surface, the guest molecule can presumably only exit the cavity through openings created by structural fluctuations of the host cluster. The kinetic lability of Ga^{III} catecholate complexes[21] enables ligands to partially dissociate from the metal ions and creates openings in the host cluster through which the guest molecules can exit and enter. The ability of the guest molecule to exit the cluster cavity is supported by competition experiments, in which stepwise replacement of Me_4N^+ for Pr_4N^+, and Et_4N^+ for Pr_4N^+, is observed by ^1H NMR spectroscopy.[28]

Mass Spectrometry of the Tetrahedral Clusters. In recent years, electrospray ionization mass spectrometry (ESI-MS) has been proven most useful in the analyses of self-assembled M_xL_y type clusters and the results obtained by ESI-MS have been regarded as indicative of the solution behavior of a species rather than gas-phase behavior.[47] We can confirm this because the results obtained by ESI-MS correlate very well with all concurrent observations made by NMR and X-ray diffractometry. Nonetheless, ESI studies of such clusters remain nontrivial. The optimization of the spectra for the $[Ti_4\mathbf{A}_4]^{8-}$ cluster has been discussed in detail.[48]

The spectrum ($MeOH:CH_3CN:H_2O$, 4:4:1, v/v/v, cation detection mode) obtained for the $[Ti_4\mathbf{A}_4]^{8-}$ cluster, as its octakis-triethylammonium salt is shown in Figure 23. Clearly observable are two main clusters of peaks corresponding to mono- and dicationic clusters, respectively. The cluster of peaks is generated by exchange of protons for (ubiquitously present) Na^+ ions. In addition, single peaks corresponding to species associated to triethylammonium ions can be identified. No peak which can be assigned to a M_xL_y species with $x,y \neq 4$ can be identified, attesting to the unique stability of the tetrahedral supramolecular assembly.

When recording the ESI spectrum of the $[Ti_4\mathbf{A}_4]^{8-}$ cluster in the negative detection mode, we were pleased to find a dramatically improved spectrum (Figure 24). The extraordinarily simple spectrum shows four main peaks, which can be assigned to the hepta- ($\{[Ti_4\mathbf{A}_4]^{8-}\cdot 7H^+\}^-$ at m/z 2300.1), hexa- ($\{[Ti_4\mathbf{A}_4]^{8-}\cdot 6H^+\}^{2-}$ at m/z 1149.6), penta- ($\{[Ti_4\mathbf{A}_4]^{8-}\cdot 5H^+\}^{3-}$ at m/z 766.1), and tetraprotonated ($\{[Ti_4\mathbf{A}_4]^{8-}\cdot 4H^+\}^{4-}$ at m/z 574.3) anion. This assignment was corroborated by the zoom scans over the narrow mass range of interest (inserts in Figure 24). The peak separation within the multiply charged clusters are, as indicated by the charge state of the ion generating the pattern, separated by $^1/_2$, $^1/_3$ and $^1/_4$ Da, respectively. The presence of up to a heptaprotonated metal−ligand complex without the observation of any fragmentation may seem unusual. However, the diprotonated mononuclear Ti^{IV} tris(catecholate) species is stable[49] reflecting the high stability of the Ti^{IV} tris-(catecholate) Ti−O bonds and the basicity of the resulting anionic complex. The strong association of the countercations through H-bonds to the anionic cluster was already described within the context of the description of the X-ray structure of this cluster, and we assume that, in addition to the electrostatic interactions, identical H-bonds are responsible for the adherence of the protons to the cluster, namely to the catecholate and the carbonyl oxygens. We surmise that the origin of the protons were the Et_3NH^+ countercations. Under the drying conditions following the spraying of the analyte solution into the mass spectrometer, Et_3N evaporated, leaving the protons with the anion. Consistent with the absence of solid state and NMR evidence for the presence of a host−guest complex, no ions in the mass spectrum were observed that could have indicated an encapsulated species. Again, fragmentation of the cluster under the condition of the ESI-MS was not observed.

The ESI spectrum (anion detection) exhibited by the corresponding Sn^{IV} cluster $[Sn_4\mathbf{A}_4]^{8-}$, as its triethylammonium salt, is similar to that of the Ti-analogue in that it shows a rich pattern of peaks attributable to cluster anions coordinated by x cations, resulting in various charge states ($-8 + x$), ranging from dianionic to tetraanionic, with each group of peaks modulated by proton-to-triethylammonium exchange processes. It is interesting to note that not all possible peaks attributable to this exchange process are observed. For instance, for the dicationic species, only 5 out of the 10 possibilities are observed, and only one tetraanionic species can be clearly identified.

The spectrum shown in Figure 25 was obtained from a cluster sample prepared with a slight excess of Sn^{IV}. The minor peaks at 1348.9 and 1406.4, and 2698.2 and 2813.6 m/z correspond numerically to the di- and monoanionic clusters with one and two Sn atoms as countercations, respectively, although the charge states were not confirmed in a zoom scan experiment.

(46) Perrin, C. L.; Dwyer, T. J. *Chem. Rev.* **1990**, *90*, 935−967.

(47) For examples of ESI analysis of oligonuclear metal complexes see refs 15a, 46, and (a) Marquis-Rigault, A.; Dupont-Gervais, A.; Baxter, P. N. W.; Van Dorsselaer, A.; Lehn, J.-M. *Inorg. Chem.* **1996**, *35*, 2307−2310. (b) Blanc, S.; Yakirevitch, P.; Leize, E.; Meyer, M.; Libman, J.; van Dorsselaer, A.; Albrecht-Gary, A.-M.; Shanzer, A. *J. Am. Chem. Soc.* **1997**, *119*, 4934−4944.

(48) König, S.; Brückner, C.; Raymond, K. N.; Leary, J. A. *J. Am. Soc. Mass Spectrom.* **1998**, *9*, 1099−1103.

(49) Ali, N. J.; Milne, S. J. *Br. Ceram. Trans. J.* **1987**, *86*, 113−117.

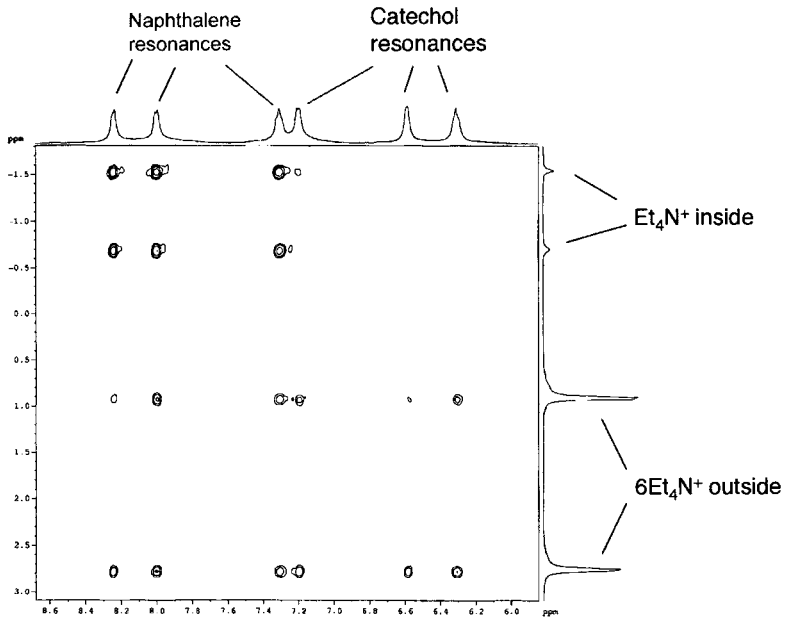

Figure 22. 2D-NOESY NMR spectrum (500 MHz, D_2O) of $K_5[Et_4N]_7[Ga_4\mathbf{C}_6]$. The horizontal axis shows the ligand resonances of the cluster, while the vertical axis shows signals corresponding to Et_4N^+.

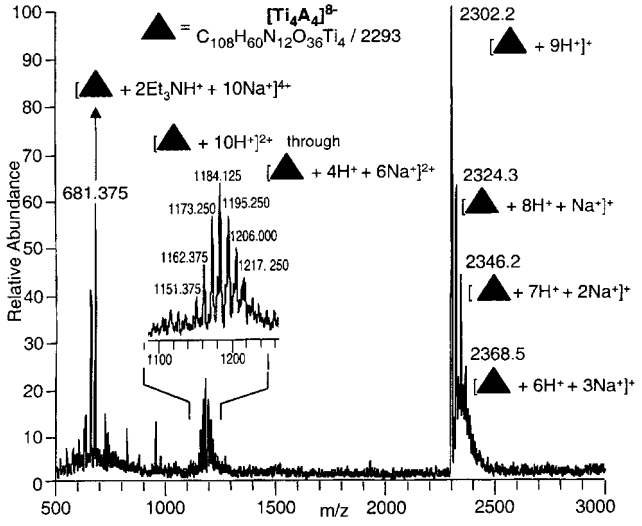

Figure 23. ES(+)-MS of $[Ti_4\mathbf{A}_4][Et_3NH]_8$. Each of the peaks in the figure insert can be assigned to a cluster dication formed from the exchange of H^+ for K^+.

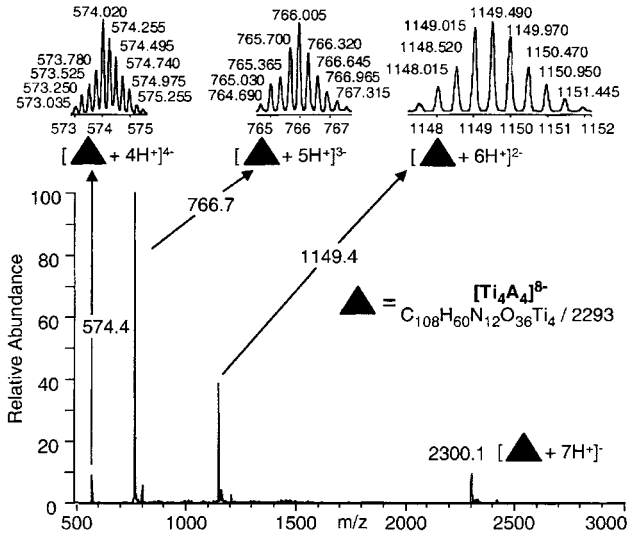

Figure 24. ES(−)-MS of $[Ti_4\mathbf{A}_4][Et_3NH]_8$. The inserts show that the charge states are confirmed for these ions using zoom scans.

Remarkably, even with an excess of metal, the cluster remains intact and non-$M_4\mathbf{A}_4$ fragments are not observed. This is a particularly powerful demonstration of the cooperative effects holding the clusters together, resulting in extraordinary stability of the tetrahedral species, and mirrors the results obtained in solution and probed by NMR.

To conclude the mass spectral results, we believe that ESI-MS allows for an unambiguous characterization of the clusters, although we found that the optimization of the spectra required the empirical variation of the spray parameters, namely the solvents and ionization conditions used.[48] Variation in the drying parameters (evaporation of the solvents) resulted in little or no changes within the parameters tested (capillary temperatures between 125 and 200 °C were probed). While it is nontrivial to infer a structure from a given composition, our data are consistent with the notion that the tetrahedral anionic structures for the complexes observed in the crystal structure are also preserved in solution under the conditions of electrospray mass spectrometry.

Conclusions

We have shown that carefully designed ligands requiring few synthetic steps can be combined with complementary metal ions to form tetrahedral tetranuclear clusters in a self-assembly process. The three design strategies outlined here are generally valid and will hopefully guide the design and synthesis of new clusters based on a variety of ligands and metals. Given the possibility of creating clusters with well-defined cavities, this seems a desirable goal in light of the rich chemistry anticipated in the inner-phase of these molecular hosts. We also anticipate that these rigid, kinetically and thermodynamically stable, metrically well-defined clusters will find a use as building blocks in nanotechnological applications.

Experimental Section

General. All NMR spectra were measured with Bruker 300, 400, or 500 MHz spectrometers. Chemical shifts are reported on the δ scale in ppm downfield from Na 3-(TMS)-propionate-2,2,3,3-d_4 in D_2O, from

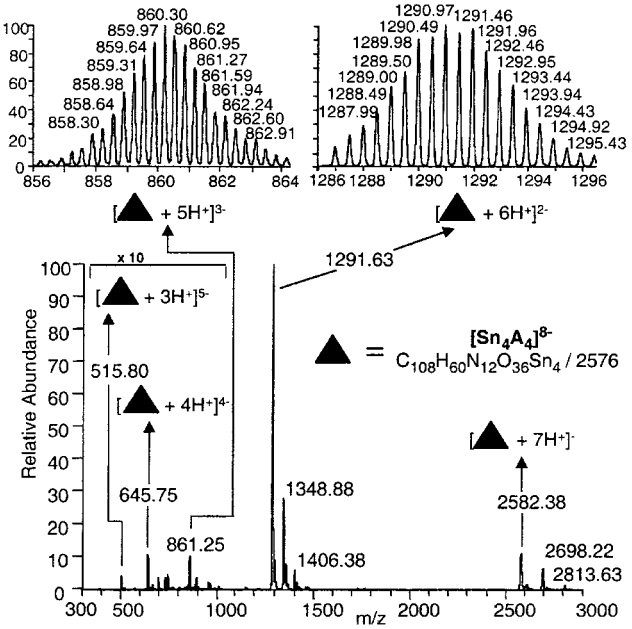

Figure 25. ESI(−)-MS of $[Sn_4\mathbf{A}_4][Et_3NH]_8$. The inserts show that the charge states are confirmed for these ions using zoom scans.

TMS in DMSO-d_6, and from the residual protic solvent peak in MeOD and DMF. Melting points are uncorrected. Elemental analyses were performed at the UCB Analytical Facilities.

Mass Spectrometry. All electrospray experiments were carried out on a Finnigan LCQ quadrupole ion trap mass spectrometer (Finnigan MAT, San Jose, CA) equipped with a microspray ionization source. Transfer lines (deactivated fused silica tubing, 40 μm and 200 μm inner diameter, polyimide coated) between the syringe pump and ion source were purchased from Polymicro (Phoenix, AZ), and all the connection pieces (Peek or stainless steel with KEL-F fittings) were obtained from Upchurch Scientific (Oak Harbor, WA). Ionization was performed under microspray conditions at a flow rate of 0.40 μL·min^{-1} and a spray voltage of 2.8−3.5 kV. For anion detection the spray voltage was set between −2.8 and −3.2 kV. All spectra were acquired at a capillary temperature of 175 °C, and all ion guide voltages were tuned to maximize the total ion current. Approximately 30 scans were averaged for a low-resolution mass spectrum, while for zoom scans, about 50 scans were averaged. The pressure inside the ion trap was 1.75^{-5} Torr or less during the acquisition (uncorrected ion gauge reading). The calibration of the extended mass range (100−4000 Da) was performed with bovine insulin (in MeOH and 2% formic acid; c = 1 pmol/μL) and NaI (in MeOH:2-propanol 1:1 (v/v), c = 0.5 mg/mL). The normal mass range (50−2000 Da) and the zoom scans were calibrated with the standard calibration procedure and compounds (caffeine, peptide MFRA, and Ultramark 1621) provided by the instrument manufacturer. Solutions of the analyte were prepared just prior to their analyses, and a concentration of 250 pmol/μL was used for all experiments.

NMR Studies. The variable-temperature NMR study was done on a 500 MHz Bruker DRX spectrometer by heating the sample from room temperature, cooling the sample back to starting temperature, and recording the spectra, producing identical results. The accuracy of the temperature was ±0.1 K. For the 2D NOESY experiment, 1 × 10^{-6} mol of $K_5[Et_4N]_7[Ga_4\mathbf{C}_6]$ was dissolved in 600 μL of D_2O. The spectrum was measured at 300 K on a 500 MHz Bruker DRX spectrometer using a NOESY sequence, with $d1$ = 2s and $d8$ = 100 ms.

General Procedure for the Formation of the Protected Ligands Me_6A, Me_4B, and Me_4C. The amines of choice (**1**, **2**, or **3**) and 1.1 equiv (based on the number of amine functionalities) of 2,3-dimethoxybenzoyl chloride (**4**) were dissolved in CH_2Cl_2 (∼10 mmol amine per 100 mL). Stoichiometric excess Et_3N was added, and the reaction mixture was stirred for several hours. The solution was washed with portions of 1 N HCl, followed by 1 N NaOH and finally water. The organic layer was isolated, dried over $MgSO_4$, and concentrated by rotary evaporation. Diethyl ether was added to precipitate the product as tan to white crystalline precipitates, which were collected by filtration and air-dried.

1,3,5-Tris(2,3-dimethoxybenzamido)benzene (Me_6A): prepared following the general procedure on a 50 mM scale in 88% yield. ^{1}H NMR (300 MHz, DMSO-d_6) δ 10.38 (s, 1H), 7.97 (s, 1H), 7.1−7.2 (m, 3H), 3.85 (s, 3H), 3.83 (s, 3H); ^{13}C NMR (75 MHz DMSO) δ 165.0, 152.6, 145.9, 139.5, 131.6, 124.2, 120.2, 114.6, 107.1, 61.1, 56.0. Anal. Calcd (Found) for $C_{33}H_{33}N_3O_9$: C 64.38 (63.80), H 5.40 (5.34), N 6.83 (6.55).

1,3-Bis(2,3-dimethoxybenzamido)benzene (Me_4B): prepared following the general procedure on a 50 mM scale in 91% yield. ^{1}H NMR (300 MHz, DMSO-d_6) δ 10.22 (br s, 2H), 8.25 (s, 1H), 7.48 (d, J = 7 Hz, 2H), 7.2 (m, 1H), 7.0−7.1 (m, 6H), 3.78 (s, 6H), 3.72 (s, 6H); ^{13}C NMR (75 MHz, DMSO-d_6) δ 165.6, 153.3, 146.6, 140.2, 132.2, 129.6, 124.9, 120.8, 115.9, 115.4, 61.8, 56.7. Anal. Calcd (Found) for $C_{24}H_{24}N_2O_6$: C 66.05 (65.75), H 5.54 (5.55), N 6.42 (6.29)

1,5-Bis(2,3-dimethoxybenzamido)naphthalene (Me_4C): prepared following the general procedure on a 50 mM scale in 82% yield*:* mp 208−209 °C. ^{1}H NMR (300 MHz, $CDCl_3$) δ 10.74 (s, 2H), 8.56 (d, J = 7.5 Hz, 2 H), 7.88 (m, 4H), 7.60 (t, J = 8.1 Hz, 2H), 7.26 (t, J = 8.1 Hz, 2H), 7.15 (dd, J = 1.2, 8.1 Hz, 2H), 4.09 (s, 6H), 3.90 (s, 6H). ^{13}C NMR (100 MHz, $CDCl_3$) δ (C) 163.5, 152.8, 147.4, 134.3, 127.0, 126.9; (CH) 126.7, 125.0, 123.3, 118.9, 116.7, 116.0; (CH_3) 62.1, 56.3. Anal. Calcd (Found) for $C_{28}H_{26}N_2O_6$: C 69.12 (68.94), H 5.39 (5.44), N 5.76 (5.65).

General Procedure for the Formation of the Ligands H_6A, H_4B, and H_4C. A four-fold stoichiometric excess per methoxy group of BBr_3 was added at −78 °C via syringe to a solution of the protected ligands Me_6**A,** Me_4**B**, and Me_4**C** in dry CH_2Cl_2 (∼100 mL/5 mmol ligand). The reaction mixture was allowed to warm to room temperature and stirred overnight. Workup procedure A: Volatiles were removed under vacuum, and the remaining residue was suspended in water for 2 h at 100 °C. The white precipitates were collected by filtration and dried under vacuum at 70 °C. Workup procedure B: Unreacted BBr_3 was quenched by the careful addition of MeOH. The mixture was distilled while repeatedly adding portions of fresh MeOH until the distillate were boron-free (flame test: one drop of the distillate when lit on a cotton swap does not burn green). The products precipitated as crystalline material from the reduced hot methanolic solution were filtered off and dried.

1,3,5-Tris(2,3-dihydroxybenzamido)benzene (H_6A): prepared following the general procedure (workup procedure B) on a 50 mM scale in 86% yield: dec >200 °C. ^{1}H NMR (300 MHz, DMSO-d_6) δ 11.50 (br s, 1H), 10.44 (s, 1H), 9.3 (s, 1H), 7.99 (s, 1H), 7.42 (d, 1H, J = 7.8 Hz), 6.99 (d, 1H, J = 7.8), 6.71 (t, 1H, J = 7.8 Hz); ^{13}C NMR (75 MHz DMSO) δ 167.7 (C═O), 148.2, 146.3, 138.7, 119.3, 118.8, 118.6, 117.4, 110.2. Anal. Calcd (Found) for $C_{27}H_{21}O_9N_3\cdot 3H_2O$: C 55.39 (55.53), H 4.65 (4.51), N 7.18 (7.11).

1,3-Bis(2,3-dihydroxybenzamido)benzene (H_4B): prepared following the general procedure (workup method A or B) on a 25 mM scale in 84% yield: dec >200 °C. ^{1}H NMR (400 MHz, DMSO-d_6) δ 11.6 (br s, 2H), 10.36 (s, 2H), 9.4 (br s, 2H), 8.08 (s, 1H), 7.4−7.5 (m, 4H), 7.28 (t, J = 8.1 Hz, 1H), 6.91 (d, J = 8.1 Hz, 2H), 6.70 (t, J = 8.1 Hz, 2H); ^{13}C NMR (125 MHz, DMSO-d_6) δ 167.7, 148.3, 146.3, 138.5, 129.0, 119.2, 118.7, 117.4, 117.3, 114.3. Anal. Calcd (Found) for $C_{20}H_{16}O_6N_2\cdot H_2O$: C 60.16 (60.30), H 4.24 (4.55), N 7.37 (7.03).

1,5-Bis(2,3-dihydroxybenzamido)naphthalene (H_4C): prepared following the general procedure (workup method A) on a 3 mM scale in 89% yield: mp = 298−302 °C (dec). ^{1}H NMR (400 MHz, DMSO-d_6) δ 11.93 (s, 2H), 10.91 (s, 2H), 9.52 (s, 2H), 7.92 (d, J = 8.5 Hz, 2H), 7.87 (d, J = 7.3 Hz, 2H), 7.64−7.59 (m, 4H), 7.03 (dd, J = 1.7, 7.9 Hz, 2H), 6.84 (t, J = 7.9 Hz, 2H). ^{13}C NMR (125 MHz, DMSO-d_6) δ (C) 168.4, 148.7, 146.7, 133.9, 129.5, 117.1; (CH) 126.5, 123.4, 121.0, 119.6, 119.2. FAB(+) MH^+ 431. Anal. Calcd (Found) for $C_{24}H_{18}N_2O_6$: C 66.97 (66.59), H 4.22 (4.26), N 6.51 (6.39).

$(Et_4N)_8[Ti_4A_4]$. A freshly prepared solution of 107 mg Ti(O*n*-Bu)$_4$ (3.1 × 10^{-4} mol) in MeOH (20 mL) was added to a solution of ligand H_6**A** (165 mg, 1 equiv) in a mixture of MeOH (20 mL) and Et_3N (1 mL), and the solution was stirred for 12 h at ambient temperature. The

orange gelatinous precipitate was removed by centrifugation and suspended in DMF (20 mL). The suspension was heated under N_2 to reflux for 12 h. The resulting solution was filtered through Celite and either evaporated to dryness in vacuo, to produce 190 mg of a microcrystalline solid, or MeOH vapors were allowed to diffuse into this solution at room temperature over several weeks to produce 80 mg (yield 37%, first crop) of orange cuboid crystals. ^{1}H NMR (300 MHz, DMSO-d_6) δ 11.43 (s, 1.5H, NH), 8.2 (variably br s, 1H, NH), 7.12 (d, J = 6.5 Hz, 1.5H, ArH), 6.84 (s, 1.5H, ArH), 6.45 (t, 1.5H, J = 7.8 Hz; ArH), 6.21 (d, 1.5H, J = 7.8 Hz; ArH), 3.00 (q, 5H, J = 7.3 Hz; CH_2), 1.14 (t, 9H, J = 7.3 Hz, CH_3); ^{13}C NMR (125 MHz, DMSO-d_6) δ 158.8 (C=O), 140.3, 138.7, 137.5, 118.5, 116.8, 115.4, 114.5, 112.9, 43.3, 8.3. ES(+)-MS (100% CH_3CN) (Na^+ is ubiquitously present): (◆ = $[Ti_4A_4]^{8-}$) 581 (◆ + $9Na^+$ + $4Et_3NH^+$)$^{5+}$, 620 (◆ + $4H^+$ + $8Na^+$)$^{4+}$, 681 (◆ + $10Na^+$ + $2Et_3NH^+$)$^{3+}$, 1151 (◆ + $10H^+$)$^{2+}$, 1162 (◆ + $9H^+$ + $1Na^+$)$^{2+}$, 1173 (◆ + $8H^+$ + $2Na^+$)$^{2+}$, 1184 (◆ + $7H^+$ + $3Na^+$)$^{2+}$, 1195 (◆ + $6H^+$ + $4Na^+$)$^{2+}$, 1206 (◆ + $5H^+$ + $5Na^+$)$^{2+}$, 1217 (◆ + $4H^+$ + $6Na^+$)$^{2+}$, 1228 (◆ + $3H^+$ + $7Na^+$)$^{2+}$, 2302 (◆ + $9H^+$)$^+$, 2324 (◆ + $8H^+$ + Na^+)$^+$, 2346 (◆ + $7H^+$ + $2Na^+$)$^+$, 2368 (◆ + $6H^+$ + $3Na^+$)$^+$, 2390 (◆ + $5H^+$ + $4Na^+$)$^+$, 2421 (◆ + $4H^+$ + $5Na^+$)$^+$. ES (CH_3CN:MeOH:H_2O 4:4:1 (v/v/v)) 2300.1 (◆ + $7H^+$)$^-$, 1149.6 (◆ + $6H^+$)$^{2-}$, 776.1 (◆ + $5H^+$)$^{3-}$, 574.3 (◆ + $4H^+$)$^{4-}$.

$(Et_4N)_8[Sn_4A_4]$. $SnCl_4$ (1.16 g, 4.45 mmol) was dissolved in 80 mL of DMF. Immediately, a solution of 2.364 g (4.45 mmol) of H_6**A** in 50 mL of DMF was added slowly, followed by the dropwise addition of 10 mL of Et_3N. The initially formed creamy precipitate dissolved and the mixture was heated to slow reflux under N_2 for 12 h. The cooled and now light pink solution was, if turbid, filtered through a bed of Celite and evaporated to dryness under vacuum. The resulting crystalline solid (quantitative yield) analyzed to be the cluster $(Et_4N)_8[Sn_4\mathbf{A}_4]$ together with up to 4 equiv of Et_3NHCl and, depending on the drying conditions, varying amounts of DMF. Repetitive recrystallization from DMF/MeOH provided a material largely free of Et_3NHCl (as per ^{1}H NMR integration) but which still did not provide a clean elemental analysis. ^{1}H NMR (300 MHz, DMSO-d_6) δ 11.29 (s, 1H, NH), 7.15 (d, J = 7.6 Hz, 1H, ArH), 6.88 (s, 1H, ArH), 6.63 (d, 1H, J = 7.6 Hz; ArH), 6.47 (t, 1H, J = 7.6 Hz; ArH), 2.99 (q, 4H, J = 7.3 Hz; CH_2), 1.14 (t, J = 7.3 Hz, CH_3). ^{13}C NMR (125 MHz, DMSO-d_6) δ 158.2, 141.3, 139.2, 138.1, 118.9, 116.9, 115.9, 115.1, 113.6, 46.6, 9.2. ES(+)-MS (100% CH_3OH)—only clusters of peaks with isotope distribution patterns indicative of dications could be unambiguously assigned: (◆ = $[Sn_4L_4]^{8-}$) 1799 (◆ + $10Et_3NH^+$)$^{2+}$, 1750 (◆ + $9Et_3NH^+$ + H^+)$^{2+}$, 1699 (◆ + $8Et_3NH^+$ + $2H^+$)$^{2+}$, 1648 (◆ + $7Et_3NH^+$ + $3H^+$)$^{2+}$, 1597 (◆ + $6Et_3NH^+$ + $4H^+$)$^{2+}$. ES (100% CH_3OH) several clusters of peaks with isotope distribution patterns indicative of multiply charged ions charge could be identified: (◆ = $[Sn_4A_4]^{8-}$) 1492 (◆ + $4Et_3NH^+$ + $2H^+$)$^{2-}$, 1442 (◆ + $3Et_3NH^+$ + $3H^+$)$^{2-}$, 1399 (◆ + $2Et_3NH^+$ + $3H^+$ + NH_4^+)$^{2-}$, 1391 (◆ + $2Et_3NH^+$ + $4H^+$)$^{2-}$, 1343 (◆ + Et_3NH^+ + $5H^+$)$^{2-}$, 966 (◆ + $3Et_3NH^+$ + H^+ + NH_4^+)$^{3-}$, 960 (◆ + $3Et_3NH^+$ + $2H^+$)$^{3-}$, 932 (◆ + $2Et_3NH^+$ + $2H^+$ + NH_4^+)$^{3-}$, 927 (◆ + $2Et_3NH^+$ + $3H^+$)$^{3-}$, 899 (◆ + $4H^+$ + NH_4^+)$^{3-}$, 894 (◆ + Et_3NH^+ + $4H^+$)$^{3-}$, 860 (◆ + $5H^+$)$^{3-}$, 722 (◆ + $3Et_3NH^+$ + H^+)$^{4-}$, 645 (◆ + $4H$)$^{4-}$ (weak).

$K_{12}[Ga_4B_6]$. H_4**B** (100 mg, 0.262 mmol) was dissolved in CH_3OH (15 mL) containing 1.04 mL of a solution of 0.5 M KOH in CH_3OH (0.52 mmol). To the light yellow solution, powdered $Ga(acac)_3$ (64 mg, 0.17 mmol) was added and subsequently dissolved. A white powder started precipitating after 6 h. The mixture was stirred for an additional 12 h and then was reduced to 5 mL. The powder was filtered and washed with acetone (20 mL) and dried under vacuum to yield 67 mg (50%). ^{1}H NMR (300 MHz, D_2O) δ 12.80 (s, 12H, NH), 7.60 (s, 12H, ArH), 7.09 (dd, J = 8.4, 1.5 Hz, 12H, ArH), 7.03 (t, J = 8.1 Hz, 6H, ArH), 6.34 (dd, J = 7.8, 1.5 Hz, 12H, ArH) 6.50 (t, J = 8.1 Hz, 12H, ArH), 6.04 (dd, J = 7.8, 1.5 Hz, 12H, ArH). FAB(+)-MS (NBA) ◆ = $[Ga_4\mathbf{B}_4]^{12-}$: m/z = 1503 [◆ + H^+ + $12K^+$]$^+$, 1463 [◆ + $2H^+$ + $11K^+$]$^+$, 1540 [◆ + $13K^+$]$^+$. ES(+)-MS (100% CH_3OH) m/e = 1538 [◆ + $14K^+$]$^{2+}$, 1039 [◆ + $15K^+$]$^{3+}$, 788 [◆ + $16K^+$]$^{4+}$. ES(+)-MS (100% CH_3CN) 1463.4 (◆ + $14K^+$)$^{2+}$, 988 (◆ + $15K^+$)$^{3+}$.

$K_5(Et_4N)_7[Ga_4C_6]$. Ligand H_4**C** (0.100 g, 0.232 mmol) was suspended, under oxygen-free conditions, in distilled MeOH (30 mL). A 0.497 N KOH solution in MeOH (935 μL, 0.464 mmol) was added via micropipet. The ligand dissolved after ca. 5 min with stirring, after which a 0.280 M solution of Et_4NCl in MeOH (1.660 mL, 0.465 mmol) was added via micropipet. Powdered $Ga(acac)_3$ (0.056 g, 0.15 mmol) was added to the solution. Within seconds the $Ga(acac)_3$ dissolved, and the solution changed from colorless to yellow. While the reaction mixture was stirred at room temperature overnight, the product precipitated as a yellow silky powder. This powder was isolated by ultracentrifugation and dried under vacuum (0.120 g, 0.029 mmol, 76%). ^{1}H NMR (300 MHz, D_2O) δ 13.60 (s, 12H, NH), 8.15 (d, J = 7.8 Hz, 12H, Ar_nH), 7.91 (d, J = 8.6 Hz, 12H, Ar_nH), 7.35 (dd, J = 1.5, 8.2 Hz, 12H, Ar_cH), 7.20 (t, J = 8.2 Hz, 12H, Ar_nH), 6.78 (dd, J = 1.5, 7.3 Hz, 12H, Ar_cH), 6.63 (t, J = 7.9 Hz, 12H, Ar_cH), 2.42 (q, J = 7.2 Hz, 48H, CH_2(out)), 0.68 (t, J = 7.2 Hz, 72H, CH_3(out)), −0.68 (m, 8H, CH_2(in)), −1.58 (t, J = 6.9 Hz, 12H, CH_3(in)). ^{13}C NMR (125 MHz, D_2O) δ (C) 172.4, 161.4, 157.7, 136.9, 129.4, 117.4; (CH) 129.4, 121.5, 120.3, 118.3, 117.8, 117.7; (CH_2) 54.5, 52.9; (CH_3) 9.1, 7.0. ES(−)-MS (100% CH_3OH): (◆ = $[Ga_4\mathbf{C}_6]^{12-}$) 859.4 [◆ + $4Et_4N^+$ + $2K^+$ + $2H^+$]$^{4-}$, 868.9 [◆ + $4Et_4N^+$ + $3K^+$ + $1H^+$]$^{4-}$, 882.2 [◆ + $5Et_4N^+$ + $1K^+$ + $2H^+$]$^{4-}$, 891.8 [◆ + $5Et_4N^+$ + $2K^+$ + $1H^+$]$^{4-}$, 914.8 [◆ + $6Et_4N^+$ + $1K^+$ + $1H^+$]$^{4-}$, 924.2 [◆ + $6Et_4N^+$ + $2K^+$]$^{4-}$, 937.4 [◆ + $7Et_4N^+$ + $1H^+$]$^{4-}$, 946.9 [◆ + $7Et_4N^+$ + $1K^+$]$^{4-}$, 1189.7 [◆ + $5Et_4N^+$ + $2K^+$ + $2H^+$]$^{3-}$, 1202.3 [◆ + $5Et_4N^+$ + $3K^+$ + $1H^+$]$^{3-}$, 1219.8 [◆ + $6Et_4N^+$ + $1K^+$ + $2H^+$]$^{3-}$, 1232.7 [◆ + $6Et_4N^+$ + $2K^+$ + $1H^+$]$^{3-}$, 1250.2 [◆ + $7Et_4N^+$ + $2H^+$]$^{3-}$, 1263.0 [◆ + $7Et_4N^+$ + $1K^+$ + $1H^+$]$^{3-}$, 1275.7 [◆ + $7Et_4N^+$ + $2K^+$]$^{3-}$, 1293.5 [◆ + $8Et_4N^+$ + $1H^+$]$^{3-}$, 1306.0 [◆ + $8Et_4N^+$ + $1K^+$]$^{3-}$. Anal. Calcd (Found) for $K_5Ga_4C_{200}H_{224}N_{19}O_{36}\cdot 8H_2O$: C 58.75 (58.43), H 5.92 (5.65), N 6.51 (6.19).

$K_5(Et_4N)_7[Fe_4C_6]$: prepared as in $K_5(Et_4N)_7[Ga_4C_6]$ above using Fe(acac)$_3$. The product was isolated as a dark red powder (79%). Crystals suitable for analysis by X-ray diffraction grew at room temperature over two weeks by gas-phase diffusion of acetone into a methanol/water solution of the complex. ES(−)-MS (100% CH_3OH) ◆ = $[Fe_4C_6]^{12-}$: m/z = 613.8 [◆ + $2Et_4N^+$ + $1Na^+$ + $4H^+$]$^{5-}$, 641.7 [◆ + $2Et_4N^+$ + $3K^+$ + $2Na^+$]$^{5-}$, 788.4 [◆ + $2Et_4N^+$ + $1K^+$ + $3Na^+$ + $2H^+$]$^{4-}$, 1094.5 [◆ + $2Et_4N^+$ + $5K^+$ + $2Na^+$]$^{3-}$, 1123.4 [◆ + $3Et_4N^+$ + $5K^+$ + $1H^+$]$^{3-}$, 1183.8 [◆ + $5Et_4N^+$ + $3K^+$ + $1H^+$]$^{3-}$, 1214.2 [◆ + $6Et_4N^+$ + $2K^+$ + $1H^+$]$^{3-}$, 1244.7 [◆ + $7Et_4N^+$ + $1K^+$ + $1H^+$]$^{3-}$, 1490.9 [◆ + $1Et_4N^+$ + $1K^+$ + $1Na^+$ + $7H^+$]$^{2-}$. Anal. Calcd (Found) for $K_5Fe_4C_{200}H_{224}N_{19}O_{36}\cdot 4H_2O$: C 60.65 (60.38), H 5.90 (5.83), N 6.72 (6.44).

$K_{11}(Et_4N)[Ga_4C_6]$: prepared as in $K_5(Et_4N)_7[Ga_4C_6]$ above using only 1 equiv of Et_4NCl (90%). ^{1}H NMR (500 MHz, D_2O) δ 13.55 (s, 5H, NH), 8.02 (bs, 12H, Ar_nH), 7.85 (bs, 12H, Ar_nH), 7.32 (d, 12H, J = 8.1 Hz, Ar_cH), 7.12 (bt, 12H, Ar_nH), 6.78 (d, 12H, J = 7.3 Hz, Ar_cH), 6.61 (t, 12H, J = 7.7 Hz, Ar_cH), −0.62 (q, 8H, J = 7.0 Hz, CH_2(in)), −1.54 (t, 12H, J = 7.0 Hz, CH_2(in)). ^{13}C NMR (125 MHz, D_2O) δ (C) 172.5, 161.1, 157.4, 136.6, 129.0, 117.4; (CH) 129.4, 121.5, 120.4, 118.4, 117.9, 117.6; (CH_2) 53.1; (CH_3) 6.9. Anal. Calcd (Found) for $K_{11}Ga_4C_{152}H_{104}N_{13}O_{36}\cdot 6H_2O$: C 52.08 (51.98), H 3.34 (3.38), N 5.19 (4.79).

Crystallography General. Crystal data for all structures investigated were collected using a Siemens SMART diffractometer equipped with a CCD area detector with graphite monochromated Mo Kα radiation (λ = 0.71073 Å). Frames corresponding to an arbitrary hemisphere of data were collected using ω scans of 0.3° counted for a total of 30 s (20 s for Me_6**A**) per frame at the temperatures noted. SAINT[50] and XPREP[51] were used for data reduction. Data were corrected for Lorentz and polarization effects. Crystallographic data (excluding structure factors) for the structures reported in this paper have been deposited with the Cambridge Crystallographic Data Centre as Supplementary Publication nos. CCDC-143379 (Me_6**A**), CCDC-101007 ($(Et_4N)_8[Ti_4\mathbf{A}_4]$), and CCDC-100947 ($K_5(Et_4N)_7[Fe_4\mathbf{C}_6]\cdot 8H_2O\cdot 3CH_3OH$), respectively. Copies of the data can be obtained free of charge on application to CCDC, 12 Union Road, Cambridge CB21EZ, UK (fax: (+44)(1223)336-033; e-mail: deposit@ccdc.cam.ac.uk)

(50) *SAINT: SAX Area Detector Integration Program*, V4.024; Siemens Industrial Automation, Inc.: Madison, WI, 1995.

(51) *SHELXTL Crystal Structure Determination Software Package*; Siemens Industrial Automation, Inc.: Madison, WI, 1993.

Crystallography of Me_6A. Clear blades of $H_{33}C_{33}N_3O_9$ having approximate dimensions of 0.15 × 0.10 × 0.05 mm were grown by vapor phase diffusion of Et_2O into a $CHCl_3$ solution of Me_6**A**. T = −116 °C, monoclinic, $P2_1/a$ (No. 14), a = 15.406(7) Å, b = 7.264(5) Å, c = 26.48(1) Å, β = 95.23(5)°, V = 2951(2) Å^3, Z = 4, μ = 0.10 mm^{-1}, $F(000)$ = 1296, ρ_{calcd} = 1.38 Mg m^{-3}, $2\Theta_{max}$ = 52.4°. Of the 13319 reflections collected 5648 were unique (R_{int} = 0.109). The structure was solved by direct methods (SIR92) and expanded using Fourier techniques using the teXsan[52] crystallographic software package. The O and N atoms were refined anisotropically, while the C atoms were refined isotropically. Hydrogen atoms were included at calculated positions. Final R = 0.059 for 1306 $I > 3\sigma(I)$, 241 parameters, R_w = 0.060, GOF = 1.41, min/max residual e$^-$ density = −0.29/-0.30 e$^-$/Å^3.

Crystallography of $(Et_3N)_8[Ti_4A_4]$. A red tabular crystal of dimensions 0.30 × 0.22 × 0.07 mm was grown by vapor diffusion of MeOH into a DMF solution of the complex; −103 ± 2 °C, trigonal, $R\bar{3}c$ (No. 167), with a = 22.6143(5) Å, c = 106.038(2) Å, V = 46963 Å^3, Z = 12, μ = 0.279 mm^{-1}, $F(000)$ = 19680, ρ_{calcd} = 1.32 Mg m^{-3}, $2\Theta_{max}$ = 41.6°. Of the 49921 reflections collected 6019 were unique (R_{int} = 0.090). An empirical absorption correction was applied using SADABS[53] (T_{max} = 0.74, T_{min} = 0.56). The structure was solved by direct methods (SIR92) and expanded using Fourier techniques using the teXsan[52] crystallographic software package. Final R = 0.109 for 1380 $I > 3\sigma(I)$, 271 variables, R_w = 0.120, GOF = 4.21, min/max residual density = −0.40/0.51 e$^-$/Å^3. The oxygen and titanium atoms were refined anisotropically, while other non-hydrogen atoms were refined isotropically. Hydrogen atoms were included in calculated idealized positions. All triethylammonium cations are disordered with respect to the conformation of their ethyl arms and their location in the crystal but could invariably be located in H-bond distance to the catecholate oxygens or the carbonyl oxygens; 8/3 Et_3NH^+ cations per asymmetric unit were distributed unequally over all four possible catecholate and all four possible carbonyl oxygen positions.

Crystallography of $K_5(Et_4N)_7[Fe_4C_6]\cdot 8H_2O\cdot 3CH_3OH$. A red blocky crystal of dimensions 0.25 × 0.23 × 0.10 mm was grown from the vapor diffusion of acetone into a methanol/water solution of the complex. T = −120 °C, cubic, $I\bar{4}3d$ (No. 220), a = 43.706(8) Å, V = 83488 Å^3, Z = 16, m = 0.45 mm^{-1}, $F(000)$ = 35808, ρ_{calcd} = 1.333 Mg m^{-3}, $2\theta_{max}$ = 41.67°. Of the 136092 reflections collected 7336 were unique (R_{int} = 0.214). An empirical absorption correction was applied using XPREP[49](ellipsoidal model, R_{int} = 0.036, T_{max} = 0.89, T_{min} = 0.83). The structure was solved by direct methods and was refined on F^2 using SHELXTL.[51] The iron atoms, oxygen and nitrogen atoms of the ligands, the half occupancy potassium, and the nitrogen and carbon atoms of the full occupancy Et_4N^+ counterion were refined anisotropically. Hydrogen atoms were included as riding on their respective carbon and nitrogen atoms for all but the disordered counterions and solvent. Not all carbon atoms were found for the disordered Et_4N^+ counterions. The N−C and C−C distances for these disordered ions were set to target values of 1.4 and 1.5 Å. An antibumping restraint was applied to carbons of the disordered Et_4N^+ on the interior of the tetrahedral cluster. Weighting scheme: $\{1\}/\{[\sigma^2(F_o^2) + (0.1660p)^2 + 779.98p]\}$, where $p = ((F_o^2,0)_{max} + 2F_c^2))/3$. Final $R1$ = 0.0978 for 4672 $F_o > 4\sigma(F_o)$ (4672 Friedel unique data, 542 parameters, 14 restraints, 3.75° < 2θ < 34.58°); for all 7336 data, wR_2 = 0.3288, GOF = 1.205; max/min residual density +0.62/−0.32 e Å^{-3}, Flack parameter = 0.03(5).[54]

Acknowledgment. This work was supported by NSF grant CHE-9709621 and the exchange grants NSF INT-9603212 and NATO SRG951516. J.A.L. and S.K. gratefully acknowledge an unrestricted UCB gift fund. We are most appreciative to Dr. Frederick Hollander (CHEXRAY, UCB) for his assistance with the structure determinations.

Supporting Information Available: Details of the X-ray structure solutions for compounds Me_6**A**, $(Et_4N)_8[Ti_4A_4]$, and $K_5(Et_4N)_7[Fe_4C_6]$ (CIF). This material is available free of charge via the Internet at http://pubs.acs.org.

JA0104507

(52) *teXsan: Crystal Structure Analysis Package*; Molecular Structure Corp.: The Woodlands, TX, 1992.

(53) Sheldrick, G. *SADABS, Siemens Area Detector ABSorption Correction Program*; personal communication, 1996.

(54) Flack, H. D. *Acta Crystallogr. A* **1993**, *39*, 876−881.